Red Thermally Activated Delayed Fluorescence and the Intersystem Crossing Mechanisms in Compact Naphthalimide–Phenothiazine Electron Donor/Acceptor Dyads

Geliang Tang, Andrey Sukhanov, Jianzhang Zhao, Wenbo Yang, Zhijia Wang, Qingyun Liu, Violeta Voronkova, Mariangela Di Donato, Daniel Escudero, Denis Jacquemin

Red Thermally-Activated Delayed Fluorescence and the Intersystem Crossing Mechanisms in Compact Naphthalimide-Phenothiazine Electron Donor/Acceptor Dyads

Geliang Tang,[a,§] Andrey A. Sukhanov,[b,§] Jianzhang Zhao,[a,c] Wenbo Yang,[a] Zhijia Wang,[a] Qingyun Liu,[d] Violeta K. Voronkova,[b]* Mariangela Di Donato,[e,f]* Daniel Escudero[g]* and Denis Jacquemin[h]**

[a] State Key Laboratory of Fine Chemicals, School of Chemical Engineering, Dalian University of Technology, Dalian 116024, P. R. China. E-mail: zhaojzh@dlut.edu.cn

[b] Zavoisky Physical-Technical Institute, FRC Kazan Scientific Center of RAS, Kazan 420029, Russia. E-mail: vio@kfti.knc.ru

[c] School of Chemistry and Chemical Engineering and Key Laboratory of Energy Materials Chemistry, Ministry of Education, Institute of Applied Chemistry, Xinjiang University, Urumqi 830046, China.

[d] College of Chemical and Environmental Engineering, Shandong University of Science and Technology, Qingdao 266590, P. R. China.

[e] LENS (European Labor Non-Linear Spectroscopy), Via N. Carrara 1, 50019 Sesto Fiorentino, Italy. E-mail: didonato@lens.unifi.it and [f] INO, Istituto Nazionale di Ottica Largo Enrico, Fermi 6, I-50125 Florence, Italy

[g] Department of Chemistry, KU Leuven, Celestijnenlaan 200F, B-3001 Leuven, Belgium. E-mail: daniel.escudero@kuleuven.be

[h] Laboratoire CEISAM UMR CNRS 6230, Université de Nantes, 2, rue de la Houssinière, 44322 Nantes, Cedex 3, France. E-mail: Denis.Jacquemin@univ-nantes.fr

§ G. T. and A. A. S. contributed equally to this work.

Abstract: Controlling of the electronic coupling between electron donor and acceptor subunits in a dyad is pivotal for the development of novel organic materials, for instance, thermally-activated delayed fluorescence (TADF) materials and triplet photosensitizers. Herein we prepared two compact electron donor/acceptor dyads based on phenothiazine (PTZ) and naphthalimide (NI) with different conformation restrictions induced by the C–N (**NI-N-PTZ)** or C–C (**NI-C-PTZ**) linkers. The effect of electronic coupling (matrix elements, V_{DA}) on the photophysical properties, especially the intersystem crossing (ISC) and the TADF were investigated. **NI-C-PTZ** shows stronger ground state electronic coupling (V_{DA} = 2548 cm^{-1}) as compared to **NI-N-PTZ** (V_{DA} = 870 cm^{-1}). TADF was observed only for **NI-N-PTZ** due to its smaller electronic coupling. Time-resolved electron paramagnetic resonance (TREPR) spectroscopy indicated the presence two triplet excited states and three ISC mechanisms in **NI-N-PTZ** with different electron spin polarizations (ESP): radical pair ISC (RP-ISC) and spin-orbital charge transfer ISC (SOCT-ISC) for one triplet state, and spin orbital coupling ISC (SO-ISC) for another. Moreover, for the second one, an inversion of the electron spin polarization (ESP) was observed at 0.5 – 1.1 μs delay time. **NI-N-PTZ** represents a rare example for compact electron donor/acceptor dyad showing TADF emission in the red spectral region.

1. INTRODUCTION

Tuning the excited states properties of organic chromophores is crucial for the development of various functional organic materials.[1–11] The photochemical properties of a molecular system, such as the absorption and emission wavelengths, intersystem crossing (ISC) and response to an external stimuli, can be controlled by controlling the excited states.[1] For instance, being able to control the emission of a molecule through the interaction with a specific analyte, allows for the development of fluorescent molecular probes, for which the fluorescence can be switched on by the selective interaction with specific compounds.[2,12] Likewise, controlling the triplet state of a chromophore, in terms of quantum yield and lifetimes, allows for the development of targeted (or activatable) photodynamic therapy (PDT) reagents,[13–16] phosphorescent molecular probes,[17,18] imaging reagents,[17] and more recently external stimuli-responsive triplet-triplet

annihilation (TTA) upconversion materials.[19–24] Enhancing the light absorption by maximizing the donor/acceptor interaction through a π-conjugation, is useful to develop photosensitizers for organic photovoltaics (OPV).[25,26] Charge separated states (CSS) may occur in such multi-chromophore molecular systems upon photoexcitation, as a storage of excitation energy, for which the electron transfer dynamics largely depend on the magnitude of the electronic coupling between the electron donor and acceptor, and the interplay of the different excited states of the system.[27]

There are two typical strategies for tuning the photophysical properties of organic chromophores: extension of the π-conjugation framework, or introduction of electron donating or accepting substituents on the π-conjugation framework.[26,28,29] Both methods induce significant modifications on the electronic properties of a chromophore, which reflected in changes of wavelength and band shapes in the UV–Vis absorption and luminescence spectra. Extended π-conjugation leads to a fully electronically coupled system, in which the individual properties of the different units are no longer distinguishable, the whole system becoming a *single* π-conjugation framework. On the other hand, connecting two different chromophores through saturated covalent bands yields a supramolecular system in which he chromophores retain their respective photophysical properties at the ground state.[30,31] In both cases energy and electron transfers between the components may occur upon photoexcitation. Besides the two approaches mentioned above, in which the electronic coupling between the components is either strong or negligible, another intermediate regime is much less investigated, in which a weak electronic coupling between the two components exists, and the molecular system is neither fully coupled, nor fully decoupled. A few examples of functional organic material which can be described in terms of weak electronic coupling between the two components have been reported.[32,33] The magnitude of the electronic coupling between two chromophores can be quantified through the electronic coupling matrix element, V_{DA}.[34–36]

The development of molecular systems with moderate electronic coupling between the chromophores can provide notable advances in the field of thermally-activated decay fluorescence (TADF) materials for

organic light emitting diodes (OLEDs). The production of such third generation OLEDs materials appears very promising since in these systems no precious metal atoms such as Ir(III) or Pt(II) are required to enhance the phosphorescence.[7,37–41] In most TADF systems, the electronic coupling between an electron donor and an electron acceptor is neither too strong nor too weak, such that charge separation is efficient and both forward and reverse ISC (RISC) are efficient because of the small S_1/T_1 energy gap.[38]

A precise understanding of the role played by the electronic coupling between the units in multi-chromophore compounds is also important to bring fundamental knowledge of the underlying photochemistry, notably by elucidating the interplay between V_{DA} and absorption, emission, and ISC properties of the system,[42–44] as well as the role played by photo-induced charge separation (CS) and of charge transfer (CT) states. To enhance the ISC, the typical method is attaching heavy atoms to chromophore, which leads to strong spin-orbital coupling effect, this method belongs to the so-called spin-orbital coupling ISC (SO ISC).[1] However, this approach suffers from some drawbacks, for instance the toxicity and high cost. Heavy atom-free triplet photosensitizers have been developed, based on the ISC mechanisms of n-$\pi^* \leftrightarrow$ n-π^* transitions,[45–47] exciton coupling,[48] electron spin converter,[49–53] etc. Moreover, it has been known for decades that charge recombination (CR) can induce ISC.[27,54,55] However, these conventional electron donor/acceptor systems are usually with large separation between donor and acceptor with long distance, which makes the synthesis difficult.[54] The ISC in the electron donor/acceptor dyads may occur via different mechanisms, such as radical pair ISC (RP-ISC), i.e. S_1/T_0 or $S_1/T_{\pm1}$ states mixing given the electron exchange energy is extremely small (J «1 cm^{-1}), or the recently proposed spin orbit charge transfer ISC (SOCT-ISC).[56] In donor/acceptor dyads with a short linker between the electron donor and acceptors, the RP-ISC is unlikely, due to the large electron exchange energy (J), which follows the $2J \propto V_{DA}^2$ relationship, leading to large S_1/T_1 energy gaps. Concerning the TADF materials,[57] very rarely the magnitude of the electronic coupling (V_{DA}) was used as a guideline for tuning the interaction of the electron donor/acceptor in the molecules. TADF molecules are typically based on carbazole and phenothiazine or phenoxazine

(PXZ), while the typical visible light organic chromophores, such as naphthalimide, were rarely used for TADF materials.[37] This is likely because arenes with large planar π-conjugation frameworks usually present a much lower T_1 state energy level than the CT state, which makes the RISC and TADF processes impossible.[7]

Herein we designed new compact electron donor/acceptor dyads based on phenothiazine (electron donor) and naphthalimide (electron acceptor and visible light-harvesting unit), with the aim to finely tune the electronic coupling and investigate its effect on the photophysical properties, especially the ISC of the dyads (Scheme 1). The conformation of the dyads is constrained by controlling the *steric hindrance* of the rotation around the linkers (C–C or C–N bonds). The geometrical conformation of the dyad can influence its electronic properties, e.g., in case of orthogonal geometry of the electron donor and the acceptor units, upon the occurrence of charge separation and recombination, SOCT-ISC can become very efficient.[33,45,58,59] Using steady state and time-resolved transient spectroscopies, we quantified the different electronic couplings between PTZ and NI moieties in the dyads, and we show that the photophysical properties are largely influenced by magnitude of V_{DA}. Interestingly, we observed TADF with one of the dyads, and rational its origin in terms of electronic coupling and the molecular geometry. With time-resolved electron paramagnetic resonance (TREPR) spectroscopy we confirmed the significant difference in the photophysical properties of the two dyads. The dyad showing TADF presents two triplet states, and the RP-ISC mechanism contribute to the electron spin polarization (ESP) pattern for one of the triplets. Furthermore, different ESP patterns are observed for the two triplet states, and an inversion of the ESP with increasing delay time was also observed for one of the two triplet states. The formation of two different triplet states in **NI-N-PTZ** dyad was confirmed by the calculation of two stable configurations of triplet states in this dyad. Therefore, the **NI-N-PTZ** dyad is a rare example of *compact* electron donor/acceptor dyad showing RP-ISC mechanism. For the analogue dyad showing no TADF property, RP-ISC was not observed with TREPR spectroscopy. These results are useful for fundamental photochemistry studies of the CS and charge

recombination (CR), the dynamics of CT state, intersystem crossing, as well as for development of red TADF materials.

2. EXPERIMENTAL SECTION

2.1. General Method. All the chemicals used in synthesis are analytically pure and were used as received. Solvents were dried and distilled prior to use. Fluorescence lifetimes were measured on an OB920 luminescence lifetime spectrometer (Edinburgh Instruments, UK). Optistat DN cryostat (Oxford Instruments, UK) was used for temperature-dependent absorption/fluorescence spectra measurements.

2.2. Compound NI-N-PTZ. **NI-Br** (100 mg, 0.258 mmol), phenothiazine (61.8 mg, 0.31 mmol), $Pd(OAc)_2$ (11.2 mg, 0.05 mmol) and sodium *tert*-butoxide (192.2 mg, 2 mmol) were mixed in dry toluene (5 mL). Then tri-*tert*-butylphosphine (0.23 mL, 0.10 mmol. 10% toluene solution) was added under N_2 atmosphere. The mixture was stirred for 8 h at 120 °C. After cooling, water (5 mL) was added, and the mixture was extracted with ethyl acetate (20 mL). The organic layer was separated and washed with water and brine solution (3 × 20 mL), respectively. The organic layer was dried over anhydrous Na_2SO_4 and the solvent was evaporated under reduced pressure. The crude product was purified by column chromatography (silica gel, DCM:PE = 2:1, v:v). Compound **NI-N-PTZ** was obtained as dark red solid. Yield: 98 mg (75%). ^{1}H NMR (400 MHz, $CDCl_3$): δ = 8.82 (d, 1H, J = 7.7 Hz), 8.65 (d, 1H, J = 7.3 Hz), 8.52 (d, 1H, J = 8.5 Hz), 7.94 (d, 1H, J = 7.7 Hz), 7.77–7.70 (m, 1H), 7.09 (d, 2H, J = 7.6 Hz), 6.88–6.75 (m, 4H), 6.06 (d, 2H, J = 8.3 Hz), 4.22–4.11 (m, 2H), 2.01–1.95 (m, 1H), 1.45–1.29 (m, 8H), 0.98–0.89 (m, 6H). ^{13}C NMR (125 MHz, $CDCl_3$): δ = 164.24, 163.89, 143.39, 143.23, 132.09, 131.85, 131.25, 130.32, 130.29, 129.93, 128.20, 127.08, 126.99, 123.66, 123.19, 123.14, 120.51, 115.80, 44.30, 38.02, 30.77, 28.69, 24.04, 23.13, 14.14, 10.66. MALDI–TOF–HRMS ($C_{32}H_{30}N_2O_2S^+$): calcd m/z = 506.2028; found m/z = 506.2034.

2.3. Compound NI-DPA. **NI-DPA** was synthesized with a method similar to that of **NI-N-PTZ**. The product was obtained as orange red solid. Yield: 78 mg (63 %). ^{1}H NMR (400 MHz, DMSO-d_6): δ = 8.47 (d, 1H, J = 8.1 Hz), 8.44 (d, 1H, J = 7.2 Hz), 8.16 (d, 1H, J = 8.4 Hz), 7.71–7.63 (m, 1H), 7.43 (d, 1H, J =

8.0 Hz), 7.35–7.27 (m, 4H), 7.13–7.04 (m, 2H), 7.00 (d, 4H, J = 7.8 Hz), 4.04–3.93 (m, 2H), 1.32–1.22 (m, 8H), 0.89–0.83 (m, 6H). HRMS ($C_{32}H_{32}N_2O_2 + H^+$): calcd m/z = 477.2464; found m/z = 477.2542.

2.4. Compound NI-C-PTZ. **NI-Br** (60 mg, 0.155 mmol), **3** (60 mg, 0.16 mmol) and K_2CO_3 (65 mg, 0.47 mmol) was mixed in DMF (5 mL) and water (0.52 mL). The mixture was purged with N_2 for 15 min, then $Pd(PPh_3)_4$ (10 mg, 0.009 mmol, 6 mol%) was added. The resulted mixture was stirred for 4 h at 80 °C. After cooling, water (5 mL) was added and the mixture was extracted with DCM (3 × 25 mL). The organic layers were combined and washed with brine solution (3 × 25 mL). The organic layer was dried over anhydrous Na_2SO_4 and the solvent was evaporated under reduced pressure. The crude product was purified by column chromatography (silica gel, DCM:PE = 2:3, v:v). **NI-C-PTZ** was obtained as orange solid. Yield: 35 mg (40%). ^{1}H NMR (400 MHz, $CDCl_3$): δ = 8.63–8.60 (m, 2H), 8.31 (d, 1H, J = 8.53 Hz), 7.72–7.64 (m, 2H), 7.30–7.27 (m, 2H), 7.22–7.15 (m, 2H), 7.02–6.92 (m, 3H), 4.20–3.89 (m, 4H), 2.00–1.94 (m, 1H), 1.91–1.83 (m, 2H), 1.56–1.49 (m, 3H), 1.43–1.30 (m, 8H), 1.01–0.87 (m, 8H). ^{13}C NMR (125 MHz, $CDCl_3$): δ= 164.70, 164.49, 145.80, 145.70, 144.76, 133.75, 132.85, 132.52, 131.21, 130.89, 129.98, 128.95, 128.80, 128.54, 127.56, 127.49, 126.78, 125.38, 124.25, 122.95, 122.81, 121.56, 115.61, 115.24, 47.30, 44.19, 37.96, 30.81, 29.04, 28.75, 24.12, 23.09, 20.24, 14.10, 13.85, 10.69. MALDI–TOF–HRMS ($C_{36}H_{38}N_2O_2S^+$): calcd m/z = 562.2654; found m/z = 562.2636.

2.5. Nanosecond Transient Absorption Spectroscopy. The nanosecond transient absorption spectra were studied with LP980 laser flash-photolysis spectrometer (Edinburgh Instruments, UK).The samples were purged 15 min with N_2 before measurement, and excited with a nanosecond pulsed laser (Opolette^{TM} 355II+UV nanosecond pulsed laser, OPOTEK, USA. the wavelength is tunable in the range of 200−2200 nm). The signal was digitized with a Tektronix TDS 3012B oscilloscope and the data was analyzed with LP900 software.

2.6. DFT Calculations. The geometries of the compounds in their ground state were optimized using density functional theory (DFT) with B3LYP functional and 6-31G(d) basis set. There are no imaginary

frequencies for all optimized structures. All these calculations were performed with Gaussian 09W. A smaller molecular model replacing the alkyl chains by hydrogens in **NI-N-PTZ** and **NI-C-PTZ** was used for the second-order algebraic diagrammatic construction (ADC(2)) calculations. Single-point ADC(2) calculations were done on top of the S_0 , S_1 and T_1 optimized geometries (the excited state ones optimized at the TD-PBE0/6-31+g(d) level of theory) with the TURBOMOLE V7.1 programme package. The def2-TZVP was chosen for the ADC(2) calculations. SOCs were computed using the quadratic-response (QR)-TD-DFT approach, as implemented in the Dalton program at their S_1 optimized geometries. For the latter calculations the B3LYP functional in combination to the 6-31G(d) basis set was used.[60]

3.RESULTS AND DISCUSSION

3.1. Molecular Structure Design and Synthesis. One of the critical methods to tune the magnitude of the electronic coupling (V_{DA}) between the components is to control the molecular geometry, for instance by tuning the dihedral angle between the electron donor and acceptor.[33,61] PTZ was selected as electron donor, as this moiety is known to form a stable radical cation,[30,62–64] whereas NI, which has extensively been used as a fluorophore for its robust photophysical properties.[65–68] To the best of our knowledge, the electronic coupling between NI and donor moieties was not studied before and the TADF of NI chromophore was never reported previously.[7,16,69–71]

Different linkages are used in the dyads **NI-N-PTZ** and **NI-C-PTZ** to connect the NI and the PTZ moieties, which lead to different rotation constrains (Scheme 1). Buchwald–Hartwig coupling reaction was used for the preparation of NI–PTZ dyad with C–N connection (**NI-N-PTZ** in Scheme 1). For this dyad, we anticipate an orthogonal orientation of the acceptor and donor units. Suzuki-Miyaura cross coupling reaction was used for the preparation of **NI-C-PTZ**, in which a C–C bond was used as linker. More rotational freedom is expected for **NI-C-PTZ** due to the smaller steric hindrance experienced by the two units. **NI-DPA**, **NI-Pip** and **NI-BA** were prepared as reference compounds (Scheme 1). The yields were satisfactory

and the molecular structures of the compounds were fully characterized by ^{1}H NMR, ^{13}C NMR and HR MS (see Experimental Section).

Scheme 1. Synthesis Procedures of the Compounds [a]

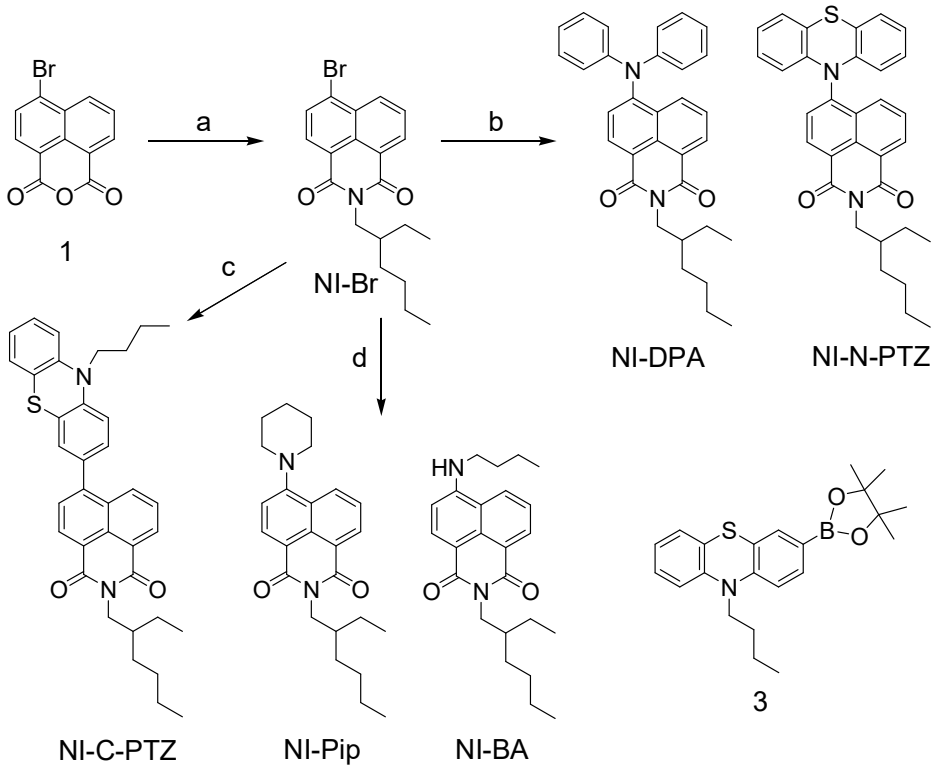

[a] Key: (a) 2-ethylhexylamine, ethanol, reflux, 6 h, yield: 74%. (b)Diphenylamine or phenothiazine, $Pd(OAc)_2$, tri-*tert*-butyl phosphine, *t*-BuONa, toluene, reflux, 9 h, yield: 63% and 75% for **NI-DPA** and **NI-N-PTZ**, respectively. (c) Compound **3**, $Pd(PPh_3)_4$, K_2CO_3, DMF, H_2O, 80 °C, 4 h, yield: 40%. (d) Piperidine or *n*-butylamine,2-methoxyethanol, reflux, 8 h, yield: 28% and 42%, respectively.

3.2. UV–Vis Absorption Spectroscopy. The UV−Vis absorption spectra of the compounds were studied (Figure 1). For **NI-Br**, the absorption maxima is at 330 nm, and the absorption band shows a clear vibrational progression. In **NI-N-PTZ**, an orthogonal orientation of the NI and the PTZ moieties is expected for the ground state geometry (see Section 3.6) and thus only a weak electronic coupling can occur between the electron donor and acceptor.[33,61] A weak, broad, and structureless absorption band in the 400 – 600 nm was observed (Figure 1a), which is interpreted as a CT transition (see Section 3.6).[33,61,72] In **NI-C-PTZ**, the rotational restriction is expected to be smaller than that in **NI-N-PTZ**, so that the two moieties adopt a more coplanar conformation, in turn yielding a significant electronic coupling between the NI and PTZ moieties.[33]

Indeed, a strong broad absorption band centered at 405 nm, assigned to a CT transition, was observed for **NI-C-PTZ** (Figure 1a). Note that this band is much more intense (ε = 9200 M^{-1} cm^{-1}) than that in **NI-N-PTZ** (ε = 600 M^{-1} cm^{-1}), hinting at a much stronger electronic coupling (V_{DA}) between the donor and the acceptor in **NI-C-PTZ**. For both **NI-N-PTZ** and **NI-C-PTZ**, the structured absorption band at 330 nm has almost the same topology as in **NI-Br**.

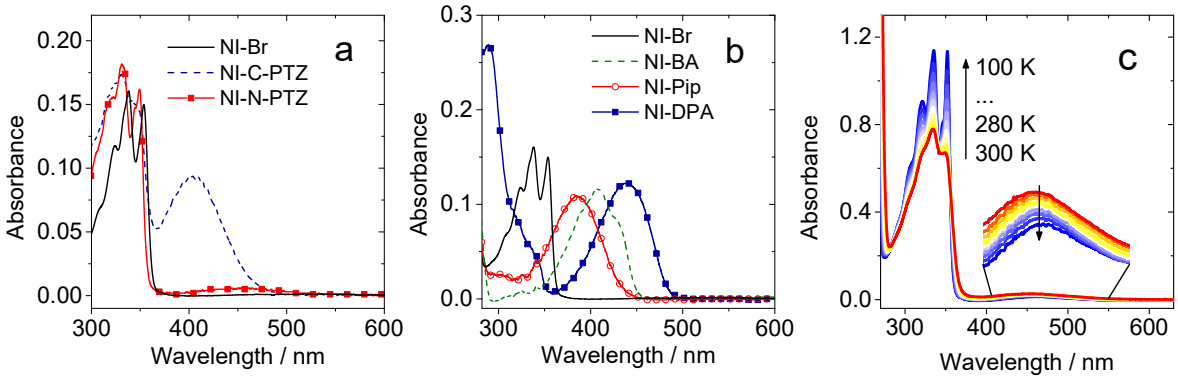

Figure 1. UV–Vis absorption spectra of (a) **NI-N-PTZ**, **NI-C-PTZ** and **NI-Br**, (b) **NI-DPA**, **NI-Pip**, **NI-BA** and **NI-Br**, c = 1.0 × 10^{-5} M in hexane, 20°C; (c) **NI-N-PTZ** at different temperature in mixed solvent of methanol/ethanol (1:4, v:v), c = 4.0 × 10^{-5} M.

The UV–Vis absorption spectra of the derivatives containing other amino substituents (**NI-BA**, **NI-Pip** and **NI-DPA**) are displayed in Figure 1b. Interestingly, the structured absorption band at 330 nm disappears in these compounds, and a broad absorption band in the 300 – 500 nm range was found. These compounds represent fully coupled systems, for which a new π-conjugation framework is established, contrasting with the above-discussed for weakly coupled systems. These analyses are supported by the shape of the molecular orbitals (*vide infra*).

Based on the absorption features, the transition dipole moments of the CT bands, as well as the electronic coupling between the electron donor and the acceptor can be calculated with Eqs. 1 and 2, respectively.[34,61]

$$\left|M_{\text{abs}}\right|^2 = \frac{3\ln 10}{8\pi^3 N_{\text{A}}} \frac{hc}{n\tilde{\nu}_{\text{CT}}} \int_{\text{band}} \varepsilon\left(\tilde{\nu}_{\text{CT}}\right) \mathrm{d}\tilde{\nu} \tag{1}$$

$$V_{\text{DA}}(\text{cm}^{-1}) = \left(\frac{2.06\times10^{-2}}{R}\right)\left(\varepsilon_{\text{max}}^{\text{CT}} \bar{\nu}_{\text{max}}^{\text{CT}} \Delta\bar{\nu}_{1/2}^{CT}\right)^{1/2} \tag{2}$$

where $\varepsilon(\tilde{\nu}_{\text{CT}})$ is the molar absorption coefficient of CT band (in M^{-1} cm^{-1}); $\tilde{\nu}_{\text{CT}}$ is the maximum of the $S_0 \rightarrow$CT band (in cm^{-1}); n, N_A, c and h are the refractive index of the solvent, the Avogadro constant (in mol^{-1}), the speed of light (cm s^{-1}) and the Planck constant (erg s), respectively; R is the distance between the center of donor and acceptor moiety (in Å); $\varepsilon_{\text{max}}^{\text{CT}}$ is the molar absorption coefficient at the maximum of CT band (in M^{-1} cm^{-1}); $\bar{\nu}_{\text{max}}^{\text{CT}}$ is absorption maximum of the CT absorption band (in cm^{-1}); $\Delta\bar{\nu}_{1/2}^{\text{CT}}$ is the full width of CT band at the half maximum (in cm^{-1}).

Table 1. Absorption Properties and Electronic Coupling Matrix Elements (V_{DA}) of the Compounds in Hexane

	$\lambda_{\text{abs}}(S_0\rightarrow\text{LE})$ [nm/eV] [a]	$\lambda_{\text{abs}}(S_0\rightarrow\text{CT})$ [nm/eV] [a]	$M_{\text{abs}}(S_0\rightarrow\text{CT})$ [D] [b]	$\Delta\mu_{11}$ [D] [c]	V_{DA} [eV] [d]	V_{DA}^* [eV] [f]
NI-N-PTZ	330 / 3.757	450 / 2.755	0.93	1.90	0.11	1.29
NI-C-PTZ	330 / 3.757	405 / 3.061	2.86	6.41	0.32	1.92
NI-DPA	289 / 4.290	440 / 2.818	3.67	7.35	0.48	1.29

[a] These maxima of the $S_0\rightarrow$LE band and the $S_0\rightarrow$CT band were obtained from the experiments. [b] Transition dipole moments of $S_0\rightarrow$CT transitions. In hexane solution. [c] Dipole-moment changes between ground and excited electronic states from TD-DFT calculations. [d] Electronic coupling matrix element between S_0 state and LE state. [f] Electronic coupling matrix element between LE state and CT state.

The estimated CT band transition dipole moments are listed in Table 1. It is clear that the transition dipole moment of **NI-C-PTZ** is much larger than that of **NI-N-PTZ**, and the same trend holds for the V_{DA}. For the compounds with significant π-conjugation between the electron donor and the NI moiety, for instance **NI-DPA**, the V_{DA} is much larger (0.48 eV). According to the Fermi golden rule, the rate of non-adiabatic electron transfer is proportional to the square of the electronic coupling matrix element between the initial

and the final states. Then, the interaction-matrix element between D^+–A^- and $(DA)^*$($V_{DA}{}^*$) can obtained by LE absorption band and CT emission band,[73] using Eq. 3:

$$k_{RAD} = \frac{64\pi^4 n^3}{3h}\left(V_{DA}{}^{*}\mu^{*}\right)^2 \frac{\nu^3}{\left(\Delta E_1 - \nu\right)^2} \tag{3}$$

where k_{RAD} and ν are the radiative rate constant (in s^{-1}) and the maximal emission wavenumber of CT fluorescence (in cm^{-1}), respectively, ΔE_1 is the energy gap between the locally excited (LE) state and the ground state (in cm^{-1}), μ^* is the transition dipole moment of the local transition $S_0 \rightarrow$LE (in D), which can be calculated using:

$$\left|\mu^{*}\right|^2 = \frac{3\ln 10}{8\pi^3 N_A}\frac{hc}{n\tilde{\nu}_{LE}}\int_{band}\varepsilon\left(\tilde{\nu}_{LE}\right)\mathrm{d}\tilde{\nu} \tag{4}$$

where $\varepsilon(\tilde{\nu}_{LE})$ is the molar absorption coefficient of LE band (in M^{-1} cm^{-1}); $\tilde{\nu}_{LE}$ is the maximum of the $S_0 \rightarrow$LE band (in cm^{-1}). As it can be seen in Table 1, the electronic coupling matrix element between the LE and CT states is larger than that between S_0 state and LE state.

Furthermore, the solvent effect on the UV–Vis absorption spectra of **NI-N-PTZ** and **NI-C-PTZ** was investigated (Supporting Information, Figure S16). The results show that the CT band of **NI-C-PTZ** is sensitive to solvent polarity, the absorbance decreases and the band is red-shifted by 831 cm^{-1} when going from apolar to polar media (Supporting Information, Figure S16b).

Varying the temperature tunes the average conformation of the dyads, as such the electronic coupling between the two units. For both **NI-N-PTZ** and **NI-C-PTZ**, their LE absorption bands (at 300 nm) show an increasing intensity when decreasing temperature (Figures 1c and S17). For the CT bands, more diverse trends can be observed. For **NI-N-PTZ**, the CT band is both red-shifted and decreased with decreasing temperatures (from 300 K to 100 K). For **NI-C-PTZ**, however, the CT band undergoes a hyperchromic

variation at lower temperature (Supporting Information, Figure S17). We tentatively attribute these changes to a variation of the molecular conformation as a function of the temperature (*vide infra*).

3.3. Fluorescence Emission: Thermally-Activated Delayed Fluorescence (TADF) in the Red Spectral Range. The fluorescence emission spectra of the compounds are shown in Figure 2. The general trend is that the dyads with strong electronic coupling between the donor and acceptor give stronger emission than those with weaker electronic coupling. For instance, **NI-Pip**, **NI-BA** and **NI-DPA** show brighter emissions in hexane than **NI-N-PTZ**. This result is in line with the electronic coupling magnitude in the dyads, and the coupling is much stronger in **NI-Pip**, **NI-BA** and **NI-DPA** than in the weakly coupled system, i.e., **NI-C-PTZ** and **NI-N-PTZ**.

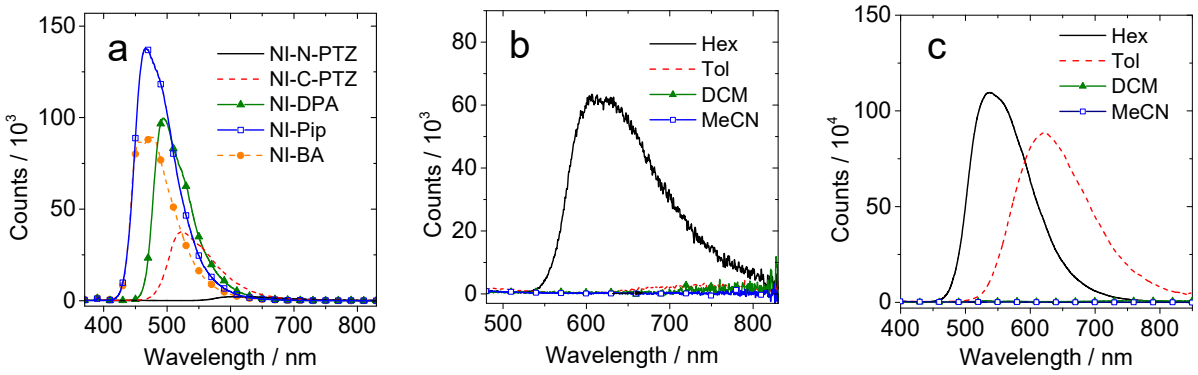

Figure 2. (a) Comparison of the fluorescence spectra of the compounds. Optically matched solutions were used, A = 0.020 at λ_{ex} = 350 nm (c = ca. 1.0 × 10^{-5} M). In hexane, 20 °C. Fluorescence emission spectra of (b) **NI-N-PTZ** and (c) **NI-C-PTZ** in different solvents. In (b) and (c) optically matched solutions were used (A = 0.166 at 330 nm, c = ca. 1.0 × 10^{-5} M). 20 °C.

The emission of **NI-N-PTZ** and **NI-C-PTZ** in different solvents were studied (Figures 2b and 2c). Interestingly, **NI-N-PTZ** shows an emission band centered at 600 nm in hexane. This broad, structureless emission band is assigned to the emissive $^1CT^*$ state, supported by TD-DFT and ADC(2) calculations (see Section 3.6).[61] No such emission band can be observed in other solvents and the fluorescence is quenched

in polar solvents. For **NI-C-PTZ**, similar emission bands were observed in hexane and toluene (Figure 2c). **NI-N-PTZ** is a weaker coupled system than **NI-C-PTZ**. As a result in solvents more polar than hexane (ε = 1.88, $E_T(30)$ = 31.0), e.g., in toluene (ε = 2.38, $E_T(30)$ = 33.0), the $^1CT^*$ will be more stabilized, and the radiative decay will be outcompeted with the non-radiative decay. In **NI-C-PTZ**, the coupling is stronger, and thus $^1CT^*$ is located higher energy than in **NI-N-PTZ**. The emission of the isolated **NI** moiety is very weak.

Table 2. Photophysical Properties of the Compounds

	λ_{abs} [nm] [a]	ε [b]	λ_{em} [nm]	τ_F [ns] [c]	τ_T [μs]	Φ_F [d]	Φ_Δ [e]
NI-N-PTZ	330	0.182	600	22.6 (97%); 2581 (3%)	2.6	0.03	0.16
NI-C-PTZ	330	0.172	522	3.9	146.1	0.36	0.10
NI-DPA	440	0.122	494	13.8	– [f]	0.70	0.00
NI-Pip	383	0.107	467	8.9	– [f]	0.67	0.00
NI-BA	408	0.111	463	10.3	– [f]	0.60	0.00

[a] Maximal UV–Vis absorption wavelength in hexane (1.0×10^{-5} M). [b] Molar absorption coefficient absorption maxima. ε: 10^5 M^{-1} cm^{-1}. [c] Fluorescence lifetime under N_2 atmosphere in hexane (1.0×10^{-5} M). [d] Absolute fluorescence quantum yield (Φ_F) (λ_{ex} = 310 nm, A = ca. 0.100) in hexane, measured with optical integration sphere. [e] Singlet oxygen ($^1O_2$) quantum yield (Φ_Δ) (λ_{ex} = 310 nm, A = 0.219) with $Ru(bpy)_3[PF_6]_2$ as standard (Φ_Δ = 0.57 in DCM) in hexane. [f] Not observed.

The photophysical properties of the compounds are summarized in Table 2. The fluorescence emission of **NI-N-PTZ** (600 nm in hexane, 2.07 eV) and **NI-C-PTZ** (522 nm in toluene, 2.38 eV) indicate that the ^1CT energy level is very close to that of the triplet state (T_1 state) of the NI chromophore (2.09 eV),[67,74,75] and thus one can envisage that the triplet state manifold can be involved in the excited state relaxation pathway. One of the typical manifestations of the interaction of emissive singlet states with triplet excited states is the occurrence of TADF, which appears following ISC from S_1 to T_1, and the subsequent thermally-activated RISC towards the S_1 state.[16,37,38,40,76]

The effect of different atmospheres on the luminescence of **NI-N-PTZ** and **NI-C-PTZ** is analyzed in Figure 3. The rationale for this kind of measurement is that the triplet state can be significantly quenched by dioxygen, O_2.[77] In contrast, the quenching of normal fluorescence by O_2 is limited, due to the spin multiplicity and the short lifetime of the singlet excited state.[77] Indeed, we found that the fluorescence of **NI-N-PTZ** is greatly quenched in aerated solution as compared to the deaerated solution. The quenching is more significant in O_2 saturated solution (Figure 3c). For **NI-C-PTZ**, however, the quenching is much weaker (Figure 3d). These results clearly suggest that the triplet excited state is involved in the fluorescence of **NI-N-PTZ** more significantly than that in **NI-C-PTZ**, hinting that the fluorescence of **NI-N-PTZ** is indeed TADF.

Next, in order to unveil the possible TADF emission of **NI-N-PTZ**, we present in Figure 3 the luminescence lifetimes under different atmospheres. Interestingly, the luminescence decay of **NI-N-PTZ** in hexane has a distinct biexponential feature, showing a fast decaying phase with a lifetime of 22.6 ns (96.6% in population) and a much longer component with a lifetime of 2.6 μs (3.4% in total population). The prompt decay component is attributed to the prompt fluorescence which is due to the direct decay from the singlet excited state. The appearance of a slow decaying component and the sensitivity of the emission intensity to O_2 unambiguously indicate the involvement of the triplet state in the luminescence of **NI-N-PTZ**, which is consistent with TADF emission.[78,81] Moreover, we assume that ISC is facilitated in **NI-N-PTZ**, due to the SOCT by the *orthogonal* molecular geometry.[33,59,82,86] The relative ratio of the prompt luminescence and the delayed fluorescence indicates that few triplet state crossed back to the emissive singlet excited states. The luminescence lifetimes of **NI-N-PTZ** under different atmospheres are summarized in Table S1. It is clear that upon deaeration, a long-lived component appeared, which is assigned to the delayed fluorescence.

For **NI-C-PTZ** we observed minor changes of the emission lifetime under different atmosphere and a single exponential decay component in deaerated solution (τ_F = 3.4 ns. Figure 3b). We thus propose that no TADF is involved in the emission of **NI-C-PTZ**. The lack of TADF in **NI-C-PTZ** is likely due to the strong

coupling between the NI and the PTZ moiety, and thus large electron exchange (J. $J \propto V_{DA}^2$) which leads to a larger S_1/T_1 energy gap ($\Delta E_{S1/T1} = 2J$), see the computed values in Section 3.6. Indeed, large S_1/T_1 energy gap is detrimental to RISC, which is crucial to TADF.[7,40,69,72] In case of **NI-C-PTZ** and other compounds, we found that the luminescence lifetimes hardly change upon deaeration, all the lifetimes are in the range of 3 – 11 ns (Supporting Information, Table S2), implying that no TADF occurs.

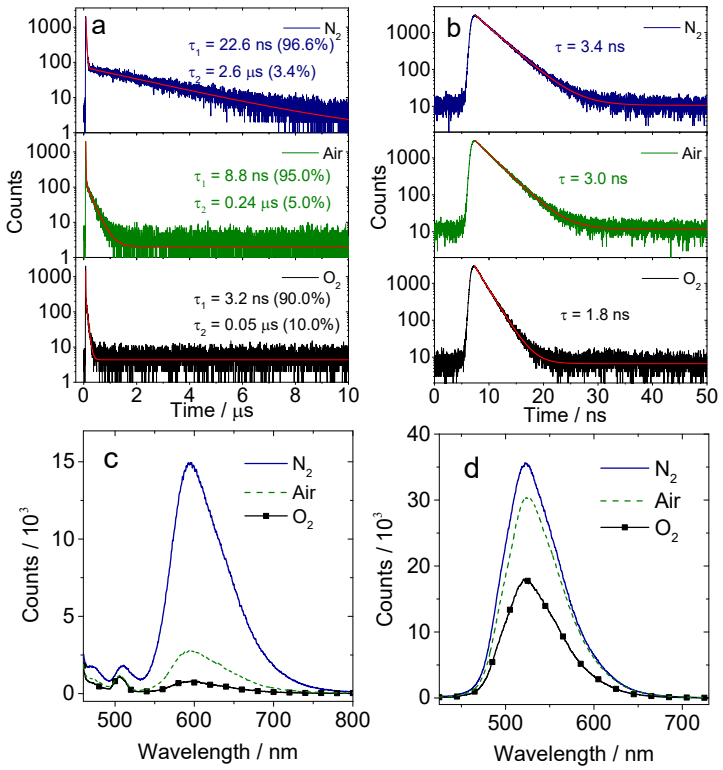

Figure 3. Fluorescence decay traces of (a) **NI-N-PTZ** (λ_{ex} = 445 nm) at 600 nm, (b) **NI-C-PTZ** (λ_{ex} = 405 nm) at 530 nm; fluorescence emission spectra of (c) **NI-N-PTZ** (λ_{ex} = 445 nm), (d) **NI-C-PTZ** (λ_{ex} = 405 nm). Under different atmospheres (N_2, air, O_2), $c = 1.0 \times 10^{-5}$ M in hexane, 20°C.

The delayed fluorescence was also observed using the laser-induced-fluorescence (LIF) mode of the LP980 laser flash photolysis spectrometer (Supporting Information, Figure S20). The luminescence lifetime (τ_1 = 22.2 ns, 79.8 % in population of the total luminescence, τ_2 = 2.4 µs, 20.2 %) is similar to that determined with the fluorescence lifetime measurements. The long-lived laser-induced fluorescence lifetime

was reduced to τ_1 = 10.1 ns (76.3 %)/ τ_2 = 264.9 ns (23.7 %) under air atmosphere, indicating the involvement of triplet state in the emission of **NI-N-PTZ**.

Delayed fluorescence can be rationalized by two mechanisms: thermally-activated delayed fluorescence (E-type delayed fluorescence), or triplet-triplet annihilation (P-type delayed fluorescence).[1,77] In order to discriminate between these two different mechanisms for **NI-N-PTZ**, the effect of concentration was studied (Supporting Information, Figures S22c and S22d). By increasing the concentration, the expected quadratic relation between emission intensity and concentration for the TTA mechanism was not observed. In contrast, a trend with downward curvature is observed (Supporting Information, Figure S22d). This result indicates that the delayed fluorescence emission is not due to TTA, but to TADF.[77] It should be noted that the triplet state lifetime of **NI-N-PTZ** is not long (2.6 μs, see later section).[74,87]

Recently, NI derivatives with carbazole moiety as electron donor were reported.[88] However, those derivatives show no TADF, although charge transfer emission was observed. The reason can be attributed to the larger S_1/T_1 energy gap for those compounds.[88] To the best of our knowledge, red emitting TADF materials, which are useful for time-resolved luminescence bioimaging, were rarely reported.[37,89,90]

The temperature-dependent luminescence spectra of **NI-N-PTZ** and **NI-C-PTZ** are shown in Figure 4. The luminescence intensity of **NI-N-PTZ** decreases upon cooling the solution from 298 K to 178 K due to the reduced thermal energy available for the reverse $T_1 \rightarrow S_1$ ISC. The normal fluorescence would intensify upon decreasing the temperature, due to the suppressed non-radiative decay processes,[1,77] which is found in **NI-C-PTZ**.

The emission of **NI-N-PTZ** is redshifted at lower temperature, which is not common in TADF materials,[91] and therefore these data were not used to derive the S_1/T_1 energy gap.[37] This phenomenon can be rationalized in terms of molecular conformation change at decreasing temperature: we expect that when lowering the temperature, the mutual orientation of the electron donor/acceptor will become more orthogonal, which

reduces the coupling between NI and PTZ moieties. As a result, a CS state will be more stabilized,[92,93] and the emission will be redshifted.

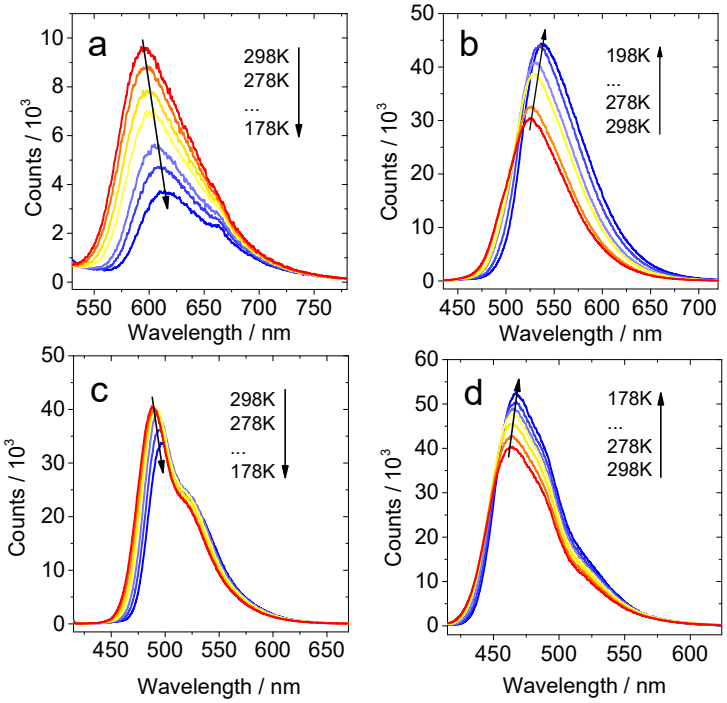

Figure 4. Temperature-dependent fluorescence emission spectra of the compounds. (a) **NI-N-PTZ**, λ_{ex} = 445 nm, (b) **NI-C-PTZ**, λ_{ex} = 405 nm, (c) **NI-DPA**, λ_{ex} = 405 nm and (d) **NI-Pip**, λ_{ex} = 405 nm. The temperature varied from 298 K to 178 K. $c = 1.0 \times 10^{-5}$ M in deaerated hexane.

3.4. Nanosecond Transient Absorption: Direct Observation of the Triplet Excited State. In order to directly confirm the population of the triplet excited state upon photoexcitation, nanosecond transient absorption spectra were recorded (Figure 5). Upon pulsed laser excitation, an excited state absorption (ESA) band centered at 420 nm was observed for **NI-N-PTZ** (Figure 5a), which is the typical feature of the triplet state absorption of NI moiety (see the ns TA of **NI-Br**, Supporting Information, Figure S27).[94] However, this band can also be assigned to the absorption of the NI radical anion, which absorbs at 420 nm ($NI^{-\bullet}$) and 491 nm.[95] These bands may also overlap with the absorption of the $PTZ^{\bullet+}$ cation, identified previously at

437 nm, 519 nm and 664 nm.[96–98] Therefore, we propose that the lowest triplet state T_1 state has LE character (^{3}NI state), but mixed with the ^{3}CT state. The determined triplet state lifetime is 2.6 µs, in agreement with the lifetime determined with the luminescence method (Table 2 and Figure 3a). This result indicates the emissive S_1 state and the dark T_1 state of **NI-N-PTZ** are in a *good equilibrium*, and

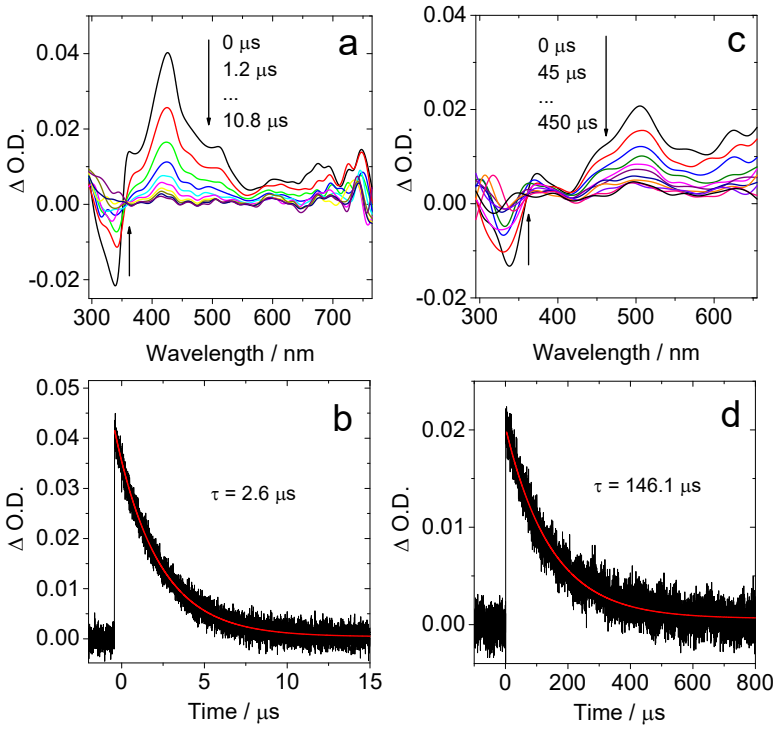

Figure 5. Nanosecond transient absorption spectra of the dyads. (a) Transient absorption spectra of **NI-N-PTZ** excited at 330 nm and (b) decay curves at 420 nm, $c = 1.0 \times 10^{-5}$ M in deaerated hexane. (c) Transient absorption spectra of **NI-C-PTZ** excited at 330 nm and (d) decay curves at 500 nm. $c = 1.0 \times 10^{-5}$ M in deaerated hexane. 20°C.

that the energy gap between the S_1 and T_1 state is very small.[7,16,71] In **NI-C-PTZ**, the triplet state lifetime (146.1 µs) is much longer than of **NI-N-PTZ**. However, the ΔO.D. values of **NI-C-PTZ** are only half of those of **NI-N-PTZ**, indicating that the triplet state quantum yield is only half that of **NI-N-PTZ**. No ns TA signal is observed for **NI-DPA**, indicating no significant production of long-lived triplet state for this compound. For both **NI-N-PTZ** and **NI-C-PTZ**, no triplet state formation was observed in polar solvents

such as dichloromethane and acetonitrile. This may be due to the faster charge recombination to give the ground state (S_0).

Spectroelectrochemistry was also used to confirm the absorption of the $NI^{-\bullet}$ and $PTZ^{+\bullet}$ in **NI-N-PTZ**. After applying negative potential (–1.70 V, vs $Ag/AgNO_3$) to **NI-N-PTZ**, we observed the generation of absorption bands centered at 430 nm, 503 nm, 698 nm, and 770 nm (Supporting Information, Figure S23a). According to literature reports,[95,99] these are the typical $NI^{-\bullet}$ absorption. It is similar to that obtained from nanosecond transient absorption spectra (426 nm and shoulder peak at 510 nm), which indicates that the triplet signal has a CT character. When a positive potential (0.63 V, vs $Ag/AgNO_3$) was applied to the same compound, peaks at 515 nm, 716 nm, 794 nm, and 894 nm are observed (Supporting Information, Figure S23b). It is a typical phenothiazine radical cation signal.[96,97] The peak centered at 515 nm is overlapped with $NI^{-\bullet}$ signal in the nanosecond transient absorption spectra. The above radical cation and anion signals indicate that we observed CSS in nanosecond transient absorption experiment, rather than a typical NI local triplet state. Although the single value decomposition (SVD) of **NI-N-PTZ** ns TA data gives only one species, it is not easy to clarify different triplet species by this ns TA result alone because the significant overlap of bands. Therefore, the TREPR technical was used to identify triplet species in these dyads (*vide infra*).

3.5. TREPR Study: Observation of Both SO-ISC and RP-ISC Mechanisms, and ESP Inversion of NI-N-PTZ. TREPR spectroscopy is useful for revealing the ISC mechanisms.[56,100] The width and the phase of the TREPR spectrum reflect the zero field splitting (ZFS) and the ESP of the T_1 state, respectively. The ZFS parameter *D* indicates the spatial confinement of the triplet state wave function, whereas the ESP pattern provides information regarding the ISC mechanisms. For instance, the typical ESP patterns of the triplet state accessed with SO-ISC are (*e*, *a*, *e*, *a*, *e*, *a*) or (*e, e, e, a, a, a*) at the six canonical orientations of the randomly oriented molecules, whereas a ESP pattern of the triplet state formed with the RP-ISC mechanism

(S/T_0 state mixing, for instance), is (*a*, *e*, *e*, *a*, *a*, *e*), where *a* stands for enhanced absorption transition and *e* stands for emissive transition in the TREPR spectra.

For electron donor/acceptor dyads, a few ISC mechanisms are possible, including the hyperfine coupling interaction (HFI) induced RP-ISC, via the S/T_0 states mixing, or $S/T_{\pm1}$ states mixing. In these cases, the electron spin-spin exchange should be smaller than the Zeeman splitting, $|2J| < g\beta\mathbf{B}$, and $|2J| \approx g\beta\mathbf{B}$, respectively, where g is the electronic Landé factor, β is the Bohr magneton, and **B** is the applied magnetic field. Moreover, in order to have efficient RP-ISC in the electron donor-bridge-acceptor systems, the distance between the electron donor and acceptor should usually be large to reduce the J magnitude. In

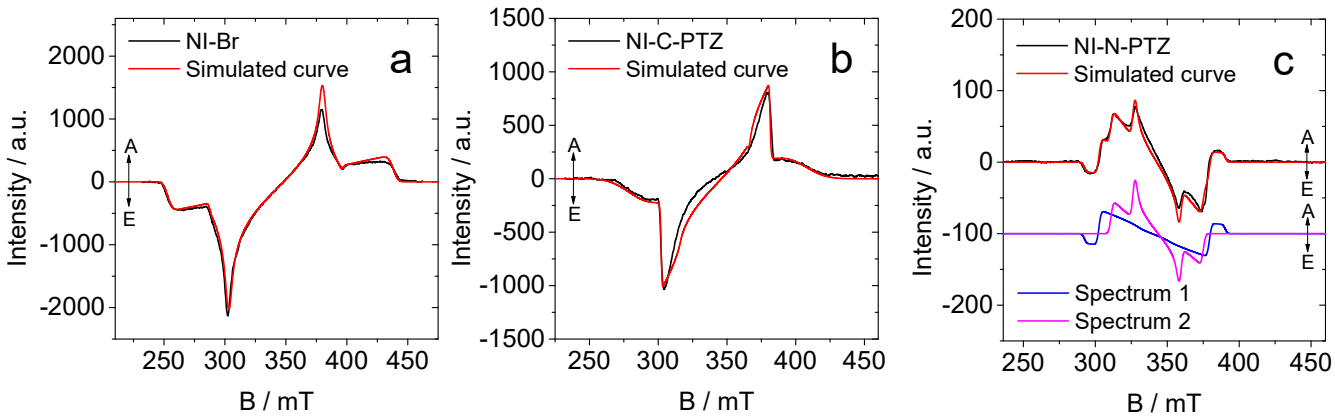

Figure 6. TREPR spectra of (a) **NI-Br**, (b) **NI-C-PTZ**, (c) **NI-N-PTZ**. Determined with X-band EPR spectrometer, at 85 K. The delay time is 0.6 – 0.7 μs following a 355 nm laser pulse, $c = 1.0 \times 10^{-3}$ M in mixed solvent hexane:toluene (1:2, v:v). Red lines are computer simulations of the triplet state spectra with parameters supplied in Table 3 for **NI-Br** and **NI-C-PTZ**. (c) The spectrum of **NI-N-PTZ** is presented as the sum of the two spectra. Details are described in the text.

molecular systems with short linkers, i.e., compact donor/acceptor dyads, $|2J| \gg g\beta\mathbf{B}$ and the RP-ISC channel is inhibited. Previously both RP-ISC and SO-ISC mechanisms were observed in perylenebisimide-Ph_n-PTZ (Ph = phenyl) systems with n >1, where n is the number of intervening phenyl linkers.[56] For systems with n

= 1, the ISC is *exclusively via* SO-ISC mechanism, no RP-ISC was observed. Compact donor/acceptor systems showing RP-ISC mechanism were rarely reported.[100]

For **NI-N-PTZ** and **NI-C-PTZ**, we observed the triplet state formation with time-resolved transient absorption spectroscopies, thus the ISC mechanisms of these dyads were studied with TREPR spectroscopy (Figure 6). The TREPR spectra of **NI-Br** and **NI-C-PTZ** are typical for randomly oriented triplet states with the (*e, a, e, a, e, a*) ESP pattern (Figure 6a and 6b). The ZFS parameters (*D* and *E*) which characterize the splitting of the triplet into three sublevels in zero magnetic field, have been determined by computer simulation (Table 3). The sign of the *D* parameter ($D > 0$) for **NI-Br** is determined from an experiment using measurements in a liquid crystal. In the remaining examples, the positive sign of the parameter is chosen by analogy.

Table 3. Zero Field Splitting Parameters (|*D*| and *E*) and Relative Population Rates p_x, p_y, p_z of the Zero Field Spin States Obtained from Simulations of the Triplet State TREPR Spectra of the Compounds

	|*D*| [MHz]	*E* [MHz]	p_z	p_y	p_x
NI-Br	2590	150	0	0.67	0.33
NI-C-PTZ	1800	140	0	0.3	0.7
NI-N-PTZ	900 [a]	0 [a]	1.0	0	0
	1380 [b]	260 [b]	0 [c]	1 [c]	0 [c]

[a] Component 2 (spectrum 2 in Figure 6c) of the TREPR spectrum of **NI-N-PTZ**, recorded with delay time of 0.6 – 0.7 μs after laser excitation. [b] Component 1 (spectrum 1 in Figure 6c) of the TREPR spectrum of **NI-N-PTZ**, recorded with delay time of 0.6 – 0.7 μs after laser excitation. [c] The population rate due to SO-ISC or SOCT-ISC mechanism contribution, main contribution from RP-ISC not shown.

The observed ESP pattern may be formed *via* a SO-ISC process. For **NI-Br**, the ISC is facilitated by the heavy atom effect of Br atom, and the triplet state is localized on **NI**. For the electron donor/acceptor dyads, it was shown that if the orientation between the electron donor and acceptor is orthogonal, and the charge

transfer between them is accompanied by a significant change in orbital angular momentum, charge recombination of the ^{1}CT state may be accompanied by an electron spin flip to directly yield triplet state.[33] Therefore the observed (*e, a, e, a, e, a*) ESP pattern and the change of population rate of the sublevels of **NI-C-PTZ** are attributed to SOCT-ISC mechanism. Although the *D* parameter and the population rate of the sublevels of **NI-C-PTZ** are different from that of **NI-Br** (Table 3), the ordinary SO-ISC mechanism cannot be also excluded for the formation of (*e, a, e, a, e, a*) ESP pattern.

The *D* parameter of **NI-C-PTZ** (1800 MHz, 0.059 cm^{-1}) is much smaller than in **NI-Br** (2590 MHz, 0.085 cm^{-1}), which may be attributed to the delocalization of the triplet state from NI moiety to PTZ moiety in **NI-C-PTZ**,[100] which is supported by the spin density isosurface studies (see later section and Supporting Information, Figure S29). The *D* parameters is also smaller than a previously determined value of the NI moiety (0.0743 cm^{-1}).[101]

Interestingly, for **NI-N-PTZ**, neither the SOCT-ISC nor the RP-ISC induced ESP *alone* can give satisfactory simulation of the experimental TREPR spectrum (Figure 6c). The analysis shows that the spectrum of **NI-N-PTZ** in Figure 6c, which was observed at delay times of 0.6 – 0.7 μs, is the sum of two spectra, i.e., spectrum 1 (blue) and spectrum 2 (pink. Figure 6c). The ESP pattern of spectrum 1 is caused by different ISC mechanisms (see analysis below), which is similar to a recent TREPR study of carbazole-derived TADF molecules.[100]

The triplet spectrum 2 (pink) of **NI-N-PTZ** (Figure 6c) shows the (*a, a, a, e, e, e*) ESP pattern. The best fit of the experimental and simulated spectra in X-band (for the spectrum recorded in Q-bands, see Supporting Information, Figure S24) gives D = 900 MHz (0.029 cm^{-1}), E = 0 MHz and preferential population to the T_z sublevel of triplet state (Table 3). We noted the different *D* values for these triplet state species, which may be due to the different confinement of the wave function of the two triplet states. With computation we found to energy minima for the T_1 state, with dihedral angles of 70° and 90 between the NI and the PTZ moieties, respectively (Supporting Information, Figure S30).

The triplet spectrum 1 (blue) of **NI-N-PTZ** (Figure 6c) shows a (*e, a, a, e, e, a*) ESP pattern, which is the unique feature of the triplet states formed by RP-ISC mechanism. Triplet spectrum 1 recorded at X-band can be simulated with the ZFS parameters of D = 1380 MHz, and E = 260 MHz. The ESP pattern and the triplet polarization ($p_z : p_y : p_x = 0 : 1 : 0$) indicates the triplet state is formed via RP-ISC. This is similar to a recently reported TREPR study of the carbazole-derived TADF compounds.[100] It should be pointed out that these results differ from the previous studies, usually indicating that RP-ISC is impossible for compact electron donor/acceptor dyads.[56] Our present results, and a recent TREPR study on TADF molecules by Ikoma et al.,[100] all show that RP-ISC is possible even in compact electron donor/acceptor dyads, probably because the geometry is close to orthogonal and the electronic coupling between the donor and acceptor is very weak. Observation of RP-ISC can be treated as a prerequisite for efficient TADF because extremely small electron exchange energy (J) leads to small ^{1}CT/^{3}CT energy gap, which is beneficial for reverse ISC (given the ^{3}LE state share similar energy level with ^{3}CT state), as well as RP-ISC. It should be noted that the spectrum 1 is very weakly manifested in the Q-band (Supporting Information, Figure S24). This confirms that the spin polarization of spectra 1, (e*, a, a, e, e, a*), is due to the RP-ISC mechanism, and we suppose that the RP-ISC takes place via $S_1/T_{\pm1}$ states mixing, otherwise (S_1/T_0 states mixing) according to the Zeeman splitting, it should be magnetic field-independent.

The D parameter for spectrum 1 of **NI-N-PTZ** is larger than that of spectrum 2 of this dyad (Figure 6c and Table 3), but still noticeably smaller than **NI-C-PTZ**. We assumed that the decrease of the D parameter for both spectrum 1 and spectrum 2 of **NI-N-PTZ** is the result of triplet state delocalization as compared to that of **NI-C-PTZ**.[100] These indicated that both triplet states will show charge transfer characters which confirmed by the spin density calculation (see later section and Supporting Information, Figure S31). Overall, the triplet state responsible for spectrum 2 is more delocalized than the triplet state contributes to spectrum 1 (Figure 6c). The observed D parameter is larger than the typical values for radical pairs having well-separated spin centers.[56] However, it should be pointed out that the ESP pattern of the triplet state with D = 900 MHz for **NI-N-PTZ** is due to the ordinary SO-ISC typical for transition from localized singlet to

triplet state. At the same time, we assume that there is weak contribution in the polarization pattern of spectrum 1 from the SO-ISC or SOCT-ISC mechanism. It was shown that the SOCT-ISC mechanism is effective when the orbitals of the donor and acceptor are approximately perpendicular. This suggests that the SOCT-ISC mechanism is more likely.[33] In later section we will show that there are two fully relaxed triplet state geometries of **NI-N-PTZ** and this condition is well satisfied for one of the geometries of the **NI-N-PTZ** dyad, but less ideally for second of the geometry and **NI-C-PTZ** dyad.

The profile of the TREPR spectrum of **NI-C-PTZ** remains unchanged within the detection time window of 0.6 – 3 μs. Interestingly, in contrast to this result, the TREPR spectrum of **NI-N-PTZ** changes with observation time (delay time) after the laser flash and inversion of ESP were observed (Figure 7). At early delay time (Figure 7a), the ESP of spectrum 2 of **NI-N-PTZ** is (*a, a, a, e, e, e*). The change in the polarization sign is clearly observed for signals corresponding to the *X*, *Y* canonical orientation (Figure 7). We find that

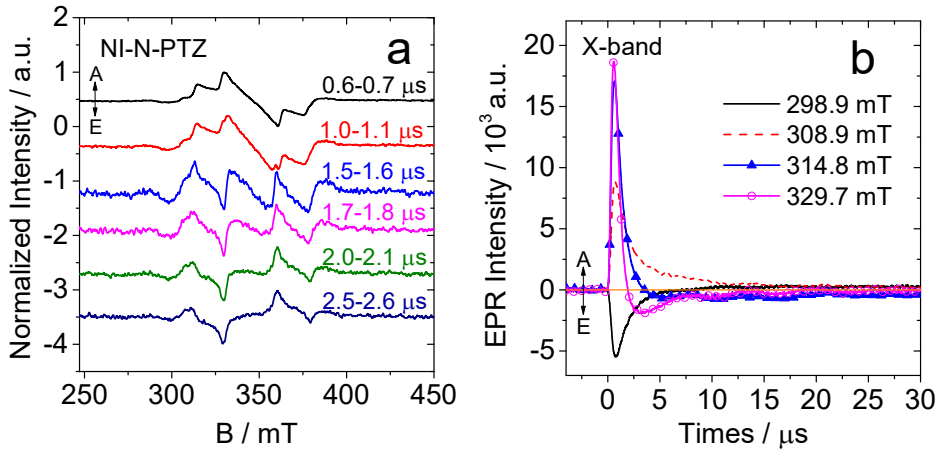

Figure 7. (a) Delay time-dependent evolution of the TREPR spectra of **NI-N-PTZ** (spectrum 2 in Figure 6c) after laser flash. (b) The time dependences of the intensity at selected magnetic fields of the X-band spectra (a).

the experimental spectrum of **NI-N-PTZ** at the delay times of 0.6 – 0.7 μs is described as the sum of two spectra 1 + 2 (Figure 6c). Changes in the total spectrum over time are mainly due to a change in the polarization sign of some signals of spectrum 2. The *D, E* parameters remain unchanged, which allows excluding any decomposition of the sample.

The time dependences of the ESP magnitude and sign at specific magnetic field strength of the X-band spectra are presented in Figure 7b. The results show that enhanced absorption (A polarization) at B = 329.7 mT changes to emission (E polarization) at longer delay time. The polarization dependence on the detection time for signals corresponding to the Z orientation is masked by signals from the spectrum 1. Inversion of populations is also evident in the spectra determined at Q-band (Supporting Information, Figure S25).

The inversion of ESP *versus* delay time for triplet excitons in phenazine-TCNQ charge transfer crystal was reported previously.[102] The authors described the ESP inversion as a result of different relaxation times and decay rates for different triplet sublevels. It was shown that this effect depends on the value of microwave power (P). This dependence is clearly observed for the triplet spectrum 2 (Supporting Information, Figure S26). Perhaps for **NI-N-PTZ**, the inversion of the ESP is result from the different decay rates of the different triplet sublevels.[103] The faster depletion of one sublevel of the triplet state, than the other two sublevels, can be used to rationalize the short triplet state lifetime of **NI-N-PTZ**.[104,105]

3.6. Theoretical Computations: Rationalization of the Photophysical Properties of the Compounds. The ground state geometries of the compounds were optimized. For **NI-N-PTZ**, the computed dihedral angle between the NI and the PTZ moieties is 85.0° (Figure 8), thus we expect a weak electronic coupling between the two moieties.[33] This is supported by the weak CT absorption band observed in the UV–Vis spectrum of **NI-N-PTZ** (Figure 1a. V_{DA} = 0.11 eV, Table 1). For **NI-C-PTZ**, the optimized geometry shows a dihedral angle of 52.8° between the PTZ and the NI moieties, and a similar dihedral angle is observed for **NI-DPA**. Therefore, a larger electronic coupling is expected for these compounds.

The molecular orbitals (MOs) of **NI-C-PTZ** and **NI-N-PTZ** are presented in Table S4 in the Supporting Information. The MOs of **NI-N-PTZ** are highly localized either on the acceptor or donor units, for instance, the HOMO and HOMO−1 are localized on the PTZ moiety. Conversely, the LUMO and LUMO+1 are confined on the NI moiety. The distribution of these frontier MOs indicates that there is little electronic coupling between the NI and PTZ moieties, consistent with experimental results.

Different results are obtained for **NI-C-PTZ**, for which the NI and PTZ moieties display significant electronic communication. For instance, the HOMO−1 of **NI-C-PTZ** is largely delocalized over PTZ and NI moieties. A similar scenario was observed for the LUMO and LUMO+1 of **NI-C-PTZ**, especially the latter (Supporting Information, Table S4). These results indicate that the electronic coupling between NI and PTZ is more significant in **NI-C-PTZ** than that in **NI-N-PTZ**, which agrees with the UV−Vis absorption observations. For **NI-DPA**, it is clear that the frontier MOs are even more delocalized than in **NI-C-PTZ** (Supporting Information, Table S4). For example, both the diphenylamine moiety and the NI moiety contribute significantly to the HOMO. Similar results were observed for **NI-Pip**.

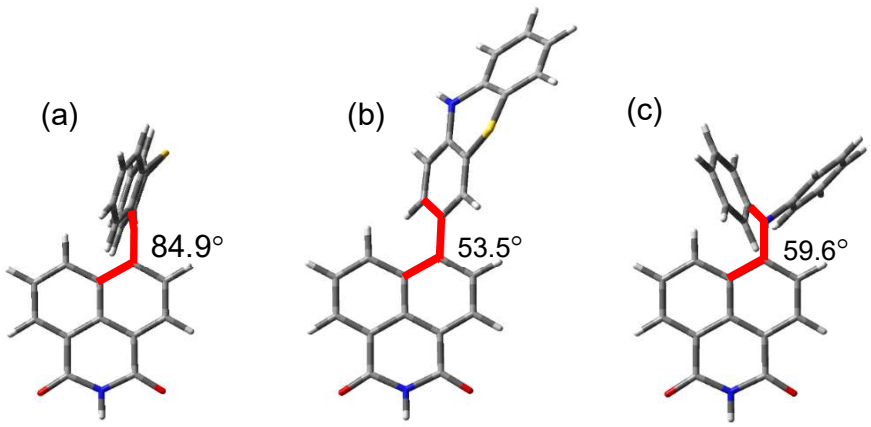

Figure 8. Dihedral angles of selected atoms of (a) **NI-N-PTZ**, (b) **NI-C-PTZ** and (c) **NI-DPA** at the optimized ground state geometries, based on the DFT-B3LYP/6-31G(d) level. Calculated with Gaussian 09W.

To simulate the UV−Vis spectra, TDDFT calculations at B3LYP/6-31G(d) level were performed. Additionally, as the latter methodology may encounter difficulties in treating CT and LE excited states in a balanced manner we have performed ADC(2)/def2-TZVP calculations as well on **NI-C-PTZ** and **NI-N-PTZ**. The TD-DFT results at the optimized ground state geometry are presented in Supporting Information (Table S5), whilst the ADC(2)/def2-TZVP results at the optimized S_0, S_1 and T_1 geometries are presented in Table 4. The experimental UV−Vis absorption maxima are well matched by the vertical ADC(2) calculations at the S_0 optimized geometries (compare, e.g., 2.76 eV vs 2.71 eV and 3.76 eV vs 3.95 eV for the CT and the LE transitions of **NI-N-PTZ**, respectively). Emission energies are also in good agreement

Table 4. ADC(2)/def2-TZVP Singlet and Triplet Electronic Transition Energies (in eV) and Oscillator Strengths (in parenthesis) of NI-N-PTZ and NI-C-PTZ at Their Optimized S_0, S_1 and T_1 Geometries; Along with SOCs (in cm^{-1}) between the Involved T_m and S_1 states

	States	S_0 geometry	S_1 geometry	T_1 geometry	$\langle S_1\|\widehat{H}_{SO}\|T_m\rangle$ [a] (Total, cm^{-1})
NI-N-PTZ	S_1	2.713 (0.0000)	1.814 (0.0000)	1.815 (0.0000)	-
	S_2	3.949 (0.3373)	3.105 (0.0003)	3.107 (0.0003)	-
	T_1	2.715 (0.0000)	1.816 (0.0000)	1.817 (0.0000)	0.004
	T_2	2.816 (0.0000)	2.499 (0.0000)	2.499 (0.0000)	0.362
NI-C-PTZ	S_1	3.273 (0.2723)	2.725 (0.0040)	2.615 (0.4936)	-
	S_2	3.799 (0.0155)	3.129 (0.0112)	3.340 (0.1588)	-
	T_1	2.708 (0.0000)	2.529 (0.0000)	2.014 (0.0000)	0.025
	T_2	3.194 (0.0000)	2.640 (0.0000)	2.729 (0.0000)	1.226

[a] Values obtained at the QR-TD-B3LYP/6-31G* level of theory at the S_1 optimized geometry. In Table 4 are also reported the SOC matrix elements between the involved excited states at the quadratic response (QR)-TD-B3LYP level of theory. SOCs estimations, unlike excitation energies, are much less dependent on the electronic structure method of choice.

with the experimental results, e.g., comparison of the experimental emission maximum at 2.07 eV to the transition computed on the optimized S_1 geometry (1.81 eV). Thus, errors in the excitation and emission energies of ca. 0.2 eV are obtained with ADC(2), but those errors are considerably larger with TD-B3LYP, e.g., an error of 0.8 eV is obtained for the CT band of **NI-N-PTZ**. Therefore, in the following, the discussion is based on the ADC(2) results.

The Jablonski energy diagram of **NI-N-PTZ** is presented in Figure 9 (the involved transitions are listed in Table 4). The S_1 state is a dark state, indicated by its negligible oscillator strength, and thus the CT absorption band of **NI-N-PTZ** is very weak. The NI-localized state is the S_2 state, and its excitation energy (3.95 eV) is close to the experimental value (3.76 eV). The geometries of the S_1 and T_1 energy minima were also optimized. Interestingly, we found that the T_1 state (1.82 eV) is adiabatically energetically aligned with the S_1 state (1.81 eV). Importantly, the $\langle S_1 | \hat{H}_{SO} | T_1 \rangle$ value is non-negligible (0.004 cm^{-1}, see Table 4). Therefore, in view of the very small singlet-triplet energy splitting and the non-negligible SOC value, the $T_1 \rightarrow S_1$ RISC is likely, which is agreement with the experimental evidences (*vide supra*). Note that higher-

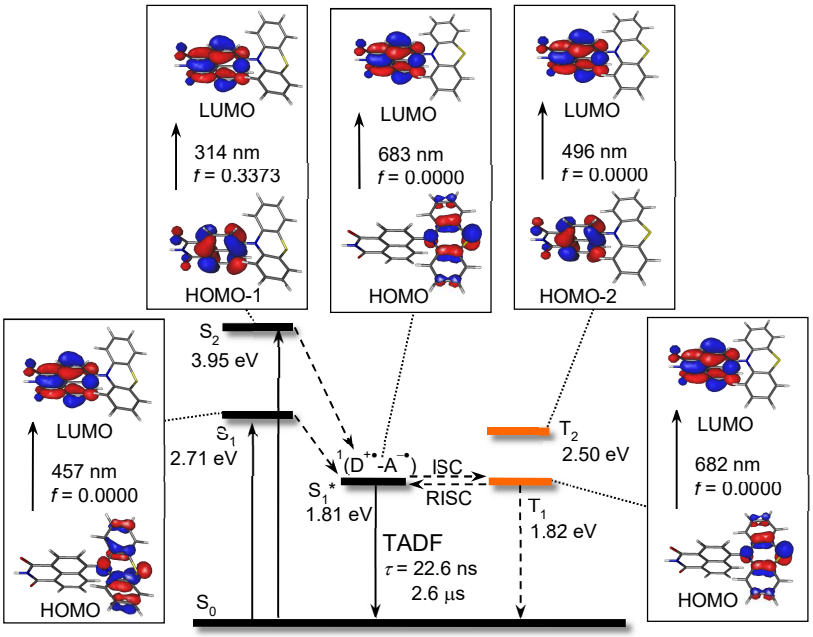

Figure 9. Jablonski energy diagram of **NI-N-PTZ** based on the computation at ADC(2) level. Alkyl chains are simplified as hydrogen atoms.

lying excited states are unlikely involved in the TADF process, as they are located > 0.5 eV above S_1 and T_1 states, both at the S_1 and T_1 optimized geometries (Table 4). Moreover, the T_1 state has CT nature mixed with LE character (^{3}CT state), in agreement with the ns TA experimental results. In addition, both the emissive S_1 state and the T_1 state have CT character, implying a slow $^1CT \rightarrow {}^3CT$ ISC, due to the lack of the coupled molecular orbital angular moment change.[54,55] Thus we expect a poor $^1CT \rightarrow {}^3CT$ efficiency, even with a small S_1/T_1 state energy gap. This is supported by the observed singlet oxygen quantum yield of **NI-N-PTZ** (16%. Table 2).

The energy diagram for **NI-C-PTZ** was also constructed (Supporting Information, Figure S28). The S_1 state has a mixed LE/CT character, and thus the $S_0 \rightarrow S_1$ is a strongly allowed transition (f = 0.2723), in contrast with the transition to S_2 state (f = 0.0155), which is of CT character. Importantly much larger S_1/T_1 energy splitting are obtained adiabatically (> 0.6 eV) as well as at the S_1 (ca. 0.20 eV) and T_1 (ca. 0.61 eV) optimized geometries. Therefore, for **NI-C-PTZ**, despite its slightly larger $\langle S_1 | \widehat{H}_{SO} | T_1 \rangle$ value, and in view of the large energy splitting, the RISC is likely not competitive to the $T_1 \rightarrow S_0$ decay. This is in agreement with the lack of TADF for this compound. $S_1 \rightarrow T_1$ ISC probably takes place via the rapid $S_1 \rightarrow T_2$ ISC process (see SOC values in Table 4).

In order to investigate the conformational flexibility of the dyads, the ground state potential energy curves of the dyads were studied (Figure 10a). There is only one energy minima for **NI-N-PTZ**, in which the two units adopt a 85° dihedral angle, i.e. a twisted geometry (orthogonal geometry). The orthogonal geometry leads to very weak coupling between the two moieties, although the thermal energy, k_BT (k_BT = 0.026 eV at room temperature, RT) induces fluctuations of the geometry to a certain extent, which may increase the coplanarity of the two components and consequently the electronic coupling. With decreasing temperature, however, the geometry fluctuations are reduced, and the molecule resides closer to the ground state optimal geometry. This reasoning explains the observations of the temperature-dependent UV–Vis absorption spectroscopy (Figure 1c). Based on the redshifts of the emission spectrum upon decreasing the temperature,

we propose a similar feature for the S_1 state (CT state) potential energy curve. Thus, at lower temperature, the electron donor and acceptor become more decoupled, the $S_1 \rightarrow S_0$ radiative transition becomes more forbidden, and its intensity decreases. This interpretation is supported by the experimental observations (Figure 4). We note that the prompt fluorescence lifetimes at RT, 21.4 ns, is prolonged to 32.7 ns at 178 K (Supporting Information, Figure S19). The potential energy curve indicates that the dihedral angle of **NI-N-PTZ** may vary in the range of 72 – 100° at RT. At 77 K, the thermal energy is 0.007 eV, the dihedral angle may vary in the range of 78 – 92° (Figure 10a). This result hints that the geometry of dyad in the excited T_1 state may vary, so that observation of T_1 states correspond more than one geometry by TREPR is possible (Figure 6c).

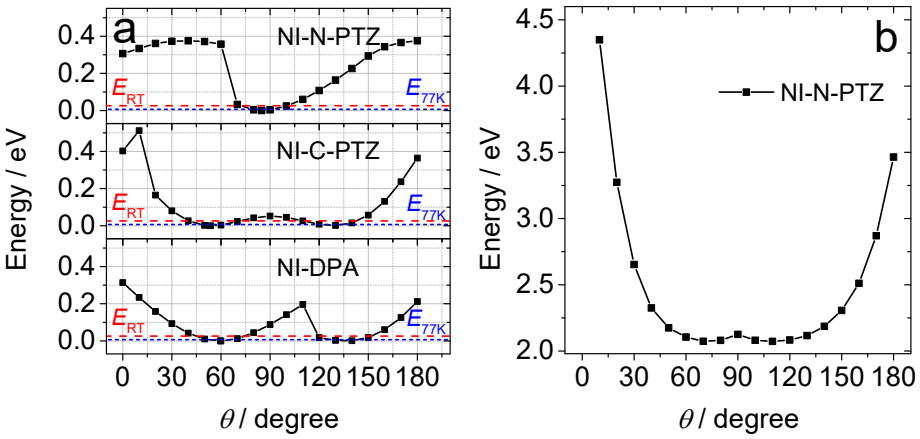

Figure 10. (a) Singlet ground state (S_0) potential energy curves of **NI-N-PTZ**, **NI-C-PTZ** and **NI-DPA**, calculated at DFT-B3LYP/6-31G(d) level. (b) Triplet excited state (T) potential energy curves of the of **NI-N-PTZ**, calculated at DFT-B3LYP/6-31G(d) level. As a function of the rotation angle (θ) between the PTZ electron donor moiety and the NI electron acceptor moiety about the C–N (for **NI-N-PTZ** and **NI-DPA**) or C–C (for **NI-C-PTZ**) bonds. Thermal energy at room temperature is marked as E_{RT} (26 meV). Thermal energy at 77 K is marked as $E_{77\,K}$ (6.6 meV).

Interestingly, there are two (almost degenerated) energy minima for **NI-C-PTZ**, with dihedral angles between the NI and the PTZ moieties at 53° and 129°, respectively. Clearly, these structures are closer to coplanar geometry, as compared to the orthogonal geometry of **NI-N-PTZ**. Moreover, the potential energy curve around the energy minima of the **NI-C-PTZ** are shallower than that of **NI-N-PTZ**. This is consistent with a stronger electronic coupling between the NI and the PTZ moieties in **NI-C-PTZ** than in **NI-N-PTZ**, in line with the spectroscopic studies. The temperature effect on the CT band of the UV−Vis absorption of **NI-C-PTZ** (Supporting Information, Figure S17) can be also rationalized by the shape of potential energy curves. Decreasing temperature will freeze the structures in either the 53° or 129° energy minima, the orthogonal geometry becoming inaccessible thermally. In these energetic minima a significant coupling between the electron donor and acceptor takes place and the CT absorption band undergoes both bathochromic and hyperchromic changes. For the **NI-N-PTZ** triplet state, full relaxation also yields two minima (Supporting Information, Figure S30), which may correspond to the formation of two different triplet states in TREPR, respectively. Interestingly, scan of the triplet state of **NI-N-PTZ** indicate the presence of two minima at ca. 70° and 90°, respectively (Figure 10b). From the spin density calculation, these two triplet minima both show charge transfer characters (Supporting Information, Figure S31), which is consist with the TREPR results.

The magnitude of the electronic coupling (J) determines the CT excitation band (**NI-N-PTZ** < **NI-C-PTZ** < **NI-DPA**) and the S_1/T_1 state energy gap ($\Delta E_{S1/T1} = 2J$). The S_1/T_1 state energy gap is very small for **NI-N-PTZ** (0.01 eV) and it increases in the order of **NI-N-PTZ** < **NI-C-PTZ** < **NI-DPA**. As such both ISC and TADF were observed for **NI-N-PTZ**, but for **NI-C-PTZ**, however, the electronic coupling is larger (V_{DA} = 0.32 eV), and the larger J value induces a larger S_1/T_1 energy gap, RISC is inhibited. Therefore, although ISC was observed, **NI-C-PTZ** is devoid of TADF. This trend strengthens further in **NI-DPA**, for which the electronic coupling is significant (0.48 eV) which makes the $S_1 \rightarrow T_1$ ISC impossible, and no triplet state production was observed for this compound. Therefore, this work proposes to tune the electronic

coupling between the electron donor/acceptor and a chromophore by controlling the molecular conformation, which finally determines the character and energy splitting of the lowest-lying excited states. This will become a powerful tool for preparing various functional organic molecules, e.g. TADF materials or heavy atom-free triplet photosensitizers.

4. CONCLUSIONS

Naphthalimide (NI)–phenothiazine (PTZ) compact electron donor/acceptor dyads were prepared, with linkage at 3-*C* or 10-*N* on the PTZ moiety, dyads **NI-N-PTZ** and **NI-C-PTZ** were obtained, respectively. Due to molecular conformation restrictions, **NI-N-PTZ** adopts a more orthogonal geometry than **NI-C-PTZ**. Thermally-activated delayed fluorescence (TADF) was observed for **NI-N-PTZ** (delayed luminescence lifetime is with biexponential feature: 22.6 ns/96.6% and 2.6 μs/3.4%, in deaerated solution), but not for **NI-C-PTZ**, as a consequence of the different electronic coupling magnitude. Calculations of excited states and potential energy curves of the rotation about the C–C/C–N linkers helped rationalizing the different electronic coupling between the NI and the PTZ moieties in the two dyads. **NI-N-PTZ** presents a weaker electronic coupling between the electron donor and acceptor (V_{DA} = 870 cm^{-1}) than that of **NI-C-PTZ** (V_{DA} = 2548 cm^{-1}). Time-resolved electron paramagnetic resonance (TREPR) studies of the triplet states of the dyads indicated two different triplet states for **NI-N-PTZ** and the three different ISC mechanisms that contribute to the electron polarization of the triplet states of **NI-N-PTZ**, i.e., SO-ISC for spectrum 2 and RP-ISC plus SOCT-ISC for spectrum 1. RP-ISC was rarely reported for *compact* electron donor/acceptor dyads. For **NI-C-PTZ**, RP-ISC was not observed. All these differences between the two dyads can be rationalized with the different electron coupling matrix elements of the **NI-N-PTZ**, and **NI-C-PTZ**, and the resultant different electron exchange energy of the charger transfer (CT) state $D^{+\bullet}$–$A^{-\bullet}$, affecting the energy gap of the S_1/T_1 states. Interestingly, inversion of the ESP of one of two triplet states was observed for **NI-N-PTZ**, but not for **NI-C-PTZ**. These results are useful for developing compact electron donor/acceptor

dyads showing efficient intersystem crossing, and study of the spin dynamics in these molecular systems, as well as for designing of novel TADF materials.

■ASSOCIATED CONTENT

Supporting Information

The Supporting Information is available free of charge on the ACS Publications website at: http://pubs.acs.org...

General information, synthesis of compounds, molecular structure characterization data, UV–Vis absorption spectra, fluorescence and lifetime spectra, spectroelectrochemistry study, time-resolved electron paramagnetic resonance spectra, nanosecond time-resolved transient absorption spectra and DFT calculation details of the compounds (PDF)

■ACKNOWLEDGEMENT

J. Zhao thank the NSFC (21673031, 21761142005 and 21911530095), the State Key Laboratory of Fine Chemicals (ZYTS201901) and the Fundamental Research Funds for the Central Universities (DUT2019TA06) for financial support. A. Sukhanov and V. Voronkova acknowledge financial support from the Government of the Russian Federation (Mega-grant No. 14.W03.31.0028) and the Russian Foundation for Basic Research (Project 19-53-53013). D. E. thanks funding from Internal Funds KU Leuven. This work used the computational resources of the CCIPL computing center installed in Nantes, France.

■REFERENCES

(1) Turro, N. J.; Ramamurthy, V.; Scaiano, J. C., *Principles of Molecular Photochemistry: An Introduction*. University Science Books: Sausalito, CA, 2009.

(2) de Silva, A. P.; Gunaratne, H. Q. N.; Gunnlaugsson, T.; Huxley, A. J. M.; McCoy, C. P.; Rademacher, J. T.; Rice, T. E. Signaling Recognition Events with Fluorescent Sensors and Switches. *Chem. Rev.* **1997**, *97*, 1515−1566.

(3) Schäferling, M. The Art of Fluorescence Imaging with Chemical Sensors. *Angew. Chem. Int. Ed.* **2012**, *51*, 3532−3554.

(4) Chen, X.; Zhou, Y.; Peng, X.; Yoon, J. Fluorescent and Colorimetric Probes for Detection of Thiols. *Chem. Soc. Rev.* **2010**, *39*, 2120−2135.

(5) Hong, Y.; Lam, J. W. Y.; Tang, B. Z. Aggregation-Induced Emission: Phenomenon, Mechanism and Applications. *Chem. Commun.* **2009**, 4332−4353.

(6) Mei, J.; Hong, Y.; Lam, J. W. Y.; Qin, A.; Tang, Y.; Tang, B. Z. Aggregation-Induced Emission: The Whole Is More Brilliant Than the Parts. *Adv. Mater.* **2014**, *26*, 5429−5479.

(7) Cao, X.; Zhang, D.; Zhang, S.; Tao, Y.; Huang, W. CN-Containing Donor-Acceptor-Type Small-Molecule Materials for Thermally Activated Delayed Fluorescence OLEDs. *J. Mater. Chem. C* **2017**, *5*, 7699−7714.

(8) Tanaka, H.; Shizu, K.; Miyazaki, H.; Adachi, C. Efficient Green Thermally Activated Delayed Fluorescence (TADF) from a Phenoxazine-Triphenyltriazine (PXZ-TRZ) Derivative. *Chem. Commun.* **2012**, *48*, 11392−11394.

(9) An, Z.; Zheng, C.; Tao, Y.; Chen, R.; Shi, H.; Chen, T.; Wang, Z.; Li, H.; Deng, R.; Liu, X., et al. Stabilizing Triplet Excited States for Ultralong Organic Phosphorescence. *Nat. Mater.* **2015**, *14*, 685−690.

(10) Wu, Y.; Xie, Y.; Zhang, Q.; Tian, H.; Zhu, W.; Li, A. D. Q. Quantitative Photoswitching in Bis(dithiazole)ethene Enables Modulation of Light for Encoding Optical Signals. *Angew. Chem. Int. Ed.* **2014**, *53*, 2090−2094.

(11) Zhu, L.; Wu, W.; Zhu, M.-Q.; Han, J. J.; Hurst, J. K.; Li, A. D. Q. Reversibly Photoswitchable Dual-Color Fluorescent Nanoparticles as New Tools for Live-Cell Imaging. *J. Am. Chem. Soc.* **2007**, *129*, 3524–3526.

(12) Cheng, T.; Xu, Y.; Zhang, S.; Zhu, W.; Qian, X.; Duan, L. A Highly Sensitive and Selective OFF-ON Fluorescent Sensor for Cadmium in Aqueous Solution and Living Cell. *J. Am. Chem. Soc.* **2008**, *130*, 16160–16161.

(13) Jiang, X.-J.; Lo, P.-C.; Yeung, S.-L.; Fong, W.-P.; Ng, D. K. P. A Ph-Responsive Fluorescence Probe and Photosensitiser Based on a Tetraamino Silicon(IV) Phthalocyanine. *Chem. Commun.* **2010**, *46*, 3188–3190.

(14) Kamkaew, A.; Lim, S. H.; Lee, H. B.; Kiew, L. V.; Chung, L. Y.; Burgess, K. Bodipy Dyes in Photodynamic Therapy. *Chem. Soc. Rev.* **2013**, *42*, 77–88.

(15) Stacey, O. J.; Pope, S. J. A. New Avenues in the Design and Potential Application of Metal Complexes for Photodynamic Therapy. *RSC Adv.* **2013**, *3*, 25550–25564.

(16) Li, X.; Kolemen, S.; Yoon, J.; Akkaya, E. U. Activatable Photosensitizers: Agents for Selective Photodynamic Therapy. *Adv. Funct. Mater.* **2017**, *27*, 1604053.

(17) Fernandez-Moreira, V.; Thorp-Greenwood, F. L.; Coogan, M. P. Application of d^6 Transition Metal Complexes in Fluorescence Cell Imaging. *Chem. Commun.* **2010**, *46*, 186–202.

(18) Zhao, Q.; Li, F.; Huang, C. Phosphorescent Chemosensors Based on Heavy-Metal Complexes. *Chem. Soc. Rev.* **2010**, *39*, 3007–3030.

(19) Cui, X.; Zhao, J.; Zhou, Y.; Ma, J.; Zhao, Y. Reversible Photoswitching of Triplet-Triplet Annihilation Upconversion Using Dithienylethene Photochromic Switches. *J. Am. Chem. Soc.* **2014**, *136*, 9256–9259.

(20) Tao, R.; Zhao, J.; Zhong, F.; Zhang, C.; Yang, W.; Xu, K. H_2O_2-Activated Triplet-Triplet Annihilation Upconversion via Modulation of the Fluorescence Quantum Yields of the Triplet Acceptor and the Triplet-Triplet-Energy-Transfer Efficiency. *Chem. Commun.* **2015**, *51*, 12403–12406.

(21) Xu, K.; Zhao, J.; Escudero, D.; Mahmood, Z.; Jacquemin, D. Controlling Triplet-Triplet Annihilation Upconversion by Tuning the PET in Aminomethyleneanthracene Derivatives. *J. Phys. Chem. C* **2015**, *119*, 23801–23812.

(22) Mahmood, Z.; Zhao, J. Thiol-Activatable Triplet-Triplet Annihilation Upconversion with Maleimide-Perylene as the Caged Triplet Acceptor/Emitter. *J. Org. Chem.* **2016**, *81*, 587–594.

(23) Mahmood, Z.; Zhao, J. The Unquenched Triplet Excited State of the Fluorescent OFF/ON Bodipy-Derived Molecular Probe Based on Photo-Induced Electron Transfer. *Photochem. Photobiol. Sci.* **2016**, *15*, 1358–1365.

(24) Xu, K.; Zhao, J.; Moore, E. G. Photo-Induced Electron Transfer in a Diamino-Substituted $Ru(bpy)_3[PF_6]_2$ Complex and Its Application as a Triplet Photosensitizer for Nitric Oxide (NO)-Activated Triplet-Triplet Annihilation Upconversion. *Photochem. Photobiol. Sci.* **2016**, *15*, 995–1005.

(25) Shen, Z.; Chen, J.; Li, X.; Li, X.; Zhou, Y.; Yu, Y.; Ding, H.; Li, J.; Zhu, L.; Hua, J. Synthesis and Photovoltaic Properties of Powerful Electron-Donating Indeno[1,2-*b*]thiophene-Based Green D–A−π–A Sensitizers for Dye-Sensitized Solar Cells. *ACS Sustainable Chem. Eng.* **2016**, *4*, 3518–3525.

(26) Wu, Y.; Zhu, W. Organic Sensitizers from D-π-A to D-A-π-A: Effect of the Internal Electron-Withdrawing Units on Molecular Absorption, Energy Levels and Photovoltaic Performances. *Chem. Soc. Rev.* **2013**, *42*, 2039–2058.

(27) Verhoeven, J. W.; van Ramesdonk, H. J.; Groeneveld, M. M.; Benniston, A. C.; Harriman, A. Long-Lived Charge-Transfer States in Compact Donor–Acceptor Dyads. *ChemPhysChem* **2005**, *6*, 2251–2260.

(28) Lu, H.; Mack, J.; Yang, Y.; Shen, Z. Structural Modification Strategies for the Rational Design of Red/NIR Region Bodipys. *Chem. Soc. Rev.* **2014**, *43*, 4778–4823.

(29) Zhang, M.; Wu, Y.; Zhang, S.; Zhu, H.; Wu, Q.; Jiao, L.; Hao, E. A Nitroolefin Functionalized Bodipy Chemodosimeter for Biothiols Driven by an Unexpected Conjugated Addition Mechanism. *Chem. Commun.* **2012**, *48*, 8925–8927.

(30) Kc, C. B.; Lim, G. N.; Nesterov, V. N.; Karr, P. A.; D'Souza, F. Phenothiazine–Bodipy–Fullerene Triads as Photosynthetic Reaction Center Models: Substitution and Solvent Polarity Effects on Photoinduced Charge Separation and Recombination. *Chem. Eur. J.* **2014**, *20*, 17100–17112.

(31) Engelhardt, V.; Kuhri, S.; Fleischhauer, J.; Garcia-Iglesias, M.; Gonzalez-Rodriguez, D.; Bottari, G.; Torres, T.; Guldi, D. M.; Faust, R. Light-Harvesting with Panchromatically Absorbing Bodipy-Porphyrazine Conjugates to Power Electron Transfer in Supramolecular Donor-Acceptor Ensembles. *Chem. Sci.* **2013**, *4*, 3888–3893.

(32) Weiss, E. A.; Ahrens, M. J.; Sinks, L. E.; Ratner, M. A.; Wasielewski, M. R. Solvent Control of Spin-Dependent Charge Recombination Mechanisms within Donor−Conjugated Bridge−Acceptor Molecules. *J. Am. Chem. Soc.* **2004**, *126*, 9510–9511.

(33) Dance, Z. E. X.; Mickley, S. M.; Wilson, T. M.; Ricks, A. B.; Scott, A. M.; Ratner, M. A.; Wasielewski, M. R. Intersystem Crossing Mediated by Photoinduced Intramolecular Charge Transfer: Julolidine−Anthracene Molecules with Perpendicular π Systems. *J. Phys. Chem. A* **2008**, *112*, 4194–4201.

(34) Pal, S. K.; Sahu, T.; Misra, T.; Ganguly, T.; Pradhan, T. K.; De, A. Synthesis, Characterization and Laser Flash Photolysis Studies of Some Naphthothiophenes Bearing Electron Donor and Acceptor Functional Groups. *J. Photochem. Photobiol. A: Chem.* **2005**, *174*, 138–148.

(35) Kim, H.; Goodson, T.; Zimmerman, P. M. Density Functional Physicality in Electronic Coupling Estimation: Benchmarks and Error Analysis. *J. Phys. Chem. Lett.* **2017**, *8*, 3242–3248.

(36) Oberhofer, H.; Blumberger, J. Electronic Coupling Matrix Elements from Charge Constrained Density Functional Theory Calculations Using a Plane Wave Basis Set. *J. Chem. Phys.* **2010**, *133*, 244105.

(37) Xiong, X.; Song, F.; Wang, J.; Zhang, Y.; Xue, Y.; Sun, L.; Jiang, N.; Gao, P.; Tian, L.; Peng, X. Thermally Activated Delayed Fluorescence of Fluorescein Derivative for Time-Resolved and Confocal Fluorescence Imaging. *J. Am. Chem. Soc.* **2014**, *136*, 9590–9597.

(38) Penfold, T. J. On Predicting the Excited-State Properties of Thermally Activated Delayed Fluorescence Emitters. *J. Phys. Chem. C* **2015**, *119*, 13535–13544.

(39) Li, M.; Liu, Y.; Duan, R.; Wei, X.; Yi, Y.; Wang, Y.; Chen, C.-F. Aromatic-Imide-Based Thermally Activated Delayed Fluorescence Materials for Highly Efficient Organic Light-Emitting Diodes. *Angew. Chem. Int. Ed.* **2017**, *56*, 8818–8822.

(40) Cui, L.-S.; Nomura, H.; Geng, Y.; Kim, J. U.; Nakanotani, H.; Adachi, C. Controlling Singlet–Triplet Energy Splitting for Deep-Blue Thermally Activated Delayed Fluorescence Emitters. *Angew. Chem. Int. Ed.* **2017**, *56*, 1571–1575.

(41) Lien, Y.-J.; Lin, T.-C.; Yang, C.-C.; Chiang, Y.-C.; Chang, C.-H.; Liu, S.-H.; Chen, Y.-T.; Lee, G.-H.; Chou, P.-T.; Lu, C.-W., et al. First N-Borylated Emitters Displaying Highly Efficient Thermally Activated Delayed Fluorescence and High-Performance OLEDs. *ACS Appl. Mater. Interfaces* **2017**, *9*, 27090–27101.

(42) Lambert, C.; Noll, G.; Schelter, J. Bridge-Mediated Hopping or Superexchange Electron-Transfer Processes in Bis(Triarylamine) Systems. *Nat. Mater.* **2002**, *1*, 69–73.

(43) Zhong, Y.-W.; Gong, Z.-L.; Shao, J.-Y.; Yao, J. Electronic Coupling in Cyclometalated Ruthenium Complexes. *Coord. Chem. Rev.* **2016**, *312*, 22–40.

(44) Heckmann, A.; Lambert, C. Organic Mixed-Valence Compounds: A Playground for Electrons and Holes. *Angew. Chem. Int. Ed.* **2012**, *51*, 326–392.

(45) Tilley, A. J.; Pensack, R. D.; Lee, T. S.; Djukic, B.; Scholes, G. D.; Seferos, D. S. Ultrafast Triplet Formation in Thionated Perylene Diimides. *J. Phys. Chem. C* **2014**, *118*, 9996–10004.

(46) Yushchenko, O.; Licari, G.; Mosquera-Vazquez, S.; Sakai, N.; Matile, S.; Vauthey, E. Ultrafast Intersystem-Crossing Dynamics and Breakdown of the Kasha–Vavilov's Rule of Naphthalenediimides. *J. Phys. Chem. Lett.* **2015**, *6*, 2096−2100.

(47) Hussain, M.; Zhao, J.; Yang, W.; Zhong, F.; Karatay, A.; Yaglioglu, H. G.; Yildiz, E. A.; Hayvali, M. Intersystem Crossing and Triplet Excited State Properties of Thionated Naphthalenediimide Derivatives. *J. Lumin.* **2017**, *192*, 211−217.

(48) Bröring, M.; Krüger, R.; Link, S.; Kleeberg, C.; Köhler, S.; Xie, X.; Ventura, B.; Flamigni, L. Bis(BF_2)-2,2′-bidipyrrins (Bisbodipys): Highly Fluorescent Bodipy Dimers with Large Stokes Shifts. *Chem. Eur. J.* **2008**, *14*, 2976−2983.

(49) Liu, Y.; Zhao, J. Visible Light-Harvesting Perylenebisimide–Fullerene (C_{60}) Dyads with Bidirectional "Ping-Pong" Energy Transfer as Triplet Photosensitizers for Photooxidation of 1,5-Dihydroxynaphthalene. *Chem. Commun.* **2012**, *48*, 3751−3753.

(50) Wu, W.; Zhao, J.; Sun, J.; Guo, S. Light-Harvesting Fullerene Dyads as Organic Triplet Photosensitizers for Triplet–Triplet Annihilation Upconversions. *J. Org. Chem.* **2012**, *77*, 5305−5312.

(51) Guo, S.; Xu, L.; Xu, K.; Zhao, J.; Küçüköz, B.; Karatay, A.; Yaglioglu, H. G.; Hayvali, M.; Elmali, A. Bodipy–C_{60} Triple Hydrogen Bonding Assemblies as Heavy Atom-Free Triplet Photosensitizers: Preparation and Study of the Singlet/Triplet Energy Transfer. *Chem. Sci.* **2015**, *6*, 3724−3737.

(52) Wang, F.; Cui, X.; Lou, Z.; Zhao, J.; Bao, M.; Li, X. Switching of the Triplet Excited State of Rhodamine-C_{60} Dyads. *Chem. Commun.* **2014**, *50*, 15627−15630.

(53) Wei, Y.; Zhou, M.; Zhou, Q.; Zhou, X.; Liu, S.; Zhang, S.; Zhang, B. Triplet–Triplet Annihilation Upconversion Kinetics of C_{60}–Bodipy Dyads as Organic Triplet Photosensitizers. *Phys. Chem. Chem. Phys.* **2017**, *19*, 22049−22060.

(54) Verhoeven, J. W. On the Role of Spin Correlation in the Formation, Decay, and Detection of Long-Lived, Intramolecular Charge-Transfer States. *J. Photochem. Photobiol. C* **2006**, *7*, 40−60.

(55) Hou, Y.; Zhang, X.; Chen, K.; Liu, D.; Wang, Z.; Liu, Q.; Zhao, J.; Barbon, A. Charge Separation, Charge Recombination, Long-Lived Charge Transfer State Formation and Intersystem Crossing in Organic Electron Donor/Acceptor Dyads. *J. Mater. Chem. C* **2019**, *7*, 12048−12074.

(56) Dance, Z. E. X.; Mi, Q.; McCamant, D. W.; Ahrens, M. J.; Ratner, M. A.; Wasielewski, M. R. Time-Resolved EPR Studies of Photogenerated Radical Ion Pairs Separated by *p*-Phenylene Oligomers and of Triplet States Resulting from Charge Recombination. *J. Phys. Chem. B* **2006**, *110*, 25163−25173.

(57) Ward, J. S.; Nobuyasu, R. S.; Batsanov, A. S.; Data, P.; Monkman, A. P.; Dias, F. B.; Bryce, M. R. The Interplay of Thermally Activated Delayed Fluorescence (TADF) and Room Temperature Organic Phosphorescence in Sterically-Constrained Donor-Acceptor Charge-Transfer Molecules. *Chem. Commun.* **2016**, *52*, 2612−2615.

(58) Okada, T.; Karaki, I.; Matsuzawa, E.; Mataga, N.; Sakata, Y.; Misumi, S. Ultrafast Intersystem Crossing in Some Intramolecular Heteroexcimers. *J. Phys. Chem.* **1981**, *85*, 3957−3960.

(59) van Willigen, H.; Jones, G.; Farahat, M. S. Time-Resolved EPR Study of Photoexcited Triplet-State Formation in Electron-Donor-Substituted Acridinium Ions. *J. Phys. Chem.* **1996**, *100*, 3312−3316.

(60) Frisch, M. J.; Trucks, G. W.; Schlegel, H. B.; Scuseria, G. E.; Robb, M. A.; Cheeseman, J. R.; Scalman, i. G.; Barone, V.; Mennucci, B.; Petersson, G. A., et al. *Gaussian 09W*, Revision A.1; Gaussian, Inc.: Wallingford, CT, 2009.

(61) Sasaki, S.; Hattori, K.; Igawa, K.; Konishi, G.-i. Directional Control of π-Conjugation Enabled by Distortion of the Donor Plane in Diarylaminoanthracenes: A Photophysical Study. *J. Phys. Chem. A* **2015**, *119*, 4898−4906.

(62) Shoer, L. E.; Eaton, S. W.; Margulies, E. A.; Wasielewski, M. R. Photoinduced Electron Transfer in 2,5,8,11-Tetrakis-Donor-Substituted Perylene-3,4:9,10-bis(dicarboximides). *J. Phys. Chem. B* **2015**, *119*, 7635−7643.

(63) Okamoto, T.; Kuratsu, M.; Kozaki, M.; Hirotsu, K.; Ichimura, A.; Matsushita, T.; Okada, K. Remarkable Structure Deformation in Phenothiazine Trimer Radical Cation. *Org. Lett.* **2004**, *6*, 3493−3496.

(64) Ajayakumar, G.; Gopidas, K. R. Long-Lived Photoinduced Charge Separation in New Ru(Bipyridine)$_3^{2+}$-Phenothiazine Dyads. *Photochem. Photobiol. Sci.* **2008**, *7*, 826−833.

(65) Wiederrecht, G. P.; Svec, W. A.; Wasielewski, M. R.; Galili, T.; Levanon, H. Triplet States with Unusual Spin Polarization Resulting from Radical Ion Pair Recombination at Short Distances. *J. Am. Chem. Soc.* **1999**, *121*, 7726−7727.

(66) Suraru, S.-L.; Würthner, F. Regioselectivity in Sequential Nucleophilic Substitution of Tetrabromonaphthalene Diimides. *J. Org. Chem.* **2013**, *78*, 5227−5238.

(67) Ventura, B.; Bertocco, A.; Braga, D.; Catalano, L.; d'Agostino, S.; Grepioni, F.; Taddei, P. Luminescence Properties of 1,8-Naphthalimide Derivatives in Solution, in Their Crystals, and in Co-Crystals: Toward Room-Temperature Phosphorescence from Organic Materials. *J. Phys. Chem. C* **2014**, *118*, 18646−18658.

(68) Doria, F.; Manet, I.; Grande, V.; Monti, S.; Freccero, M. Water-Soluble Naphthalene Diimides as Singlet Oxygen Sensitizers. *J. Org. Chem.* **2013**, *78*, 8065−8073.

(69) Tao, Y.; Yuan, K.; Chen, T.; Xu, P.; Li, H.; Chen, R.; Zheng, C.; Zhang, L.; Huang, W. Thermally Activated Delayed Fluorescence Materials Towards the Breakthrough of Organoelectronics. *Adv. Mater.* **2014**, *26*, 7931−7958.

(70) Wong, M. Y.; Zysman-Colman, E. Purely Organic Thermally Activated Delayed Fluorescence Materials for Organic Light-Emitting Diodes. *Adv. Mater.* **2017**, *29*, 1605444.

(71) Yang, Z.; Mao, Z.; Xie, Z.; Zhang, Y.; Liu, S.; Zhao, J.; Xu, J.; Chi, Z.; Aldred, M. P. Recent Advances in Organic Thermally Activated Delayed Fluorescence Materials. *Chem. Soc. Rev.* **2017**, *46*, 915−1016.

(72) Natarajan, P.; Schmittel, M. Photoluminescence, Redox Properties, and Electrogenerated Chemiluminescence of Twisted 9,9′-Bianthryls. *J. Org. Chem.* **2013**, *78*, 10383−10394.

(73) Verhoeven, J. W.; Scherer, T.; Wegewijs, B.; Hermant, R. M.; Jortner, J.; Bixon, M.; Depaemelaere, S.; de Schryver, F. C. Electronic Coupling in Inter- and Intramolecular Donor-Acceptor Systems as Revealed by Their Solvent-Dependent Charge-Transfer Fluorescence. *Recl. Trav. Chim. Pays-Bas* **1995**, *114*, 443−448.

(74) Guo, H.; Muro-Small, M. L.; Ji, S.; Zhao, J.; Castellano, F. N. Naphthalimide Phosphorescence Finally Exposed in a Platinum(II) Diimine Complex. *Inorg. Chem.* **2010**, *49*, 6802−6804.

(75) Nguyen, K. A.; Kennel, J.; Pachter, R. A Density Functional Theory Study of Phosphorescence and Triplet–Triplet Absorption for Nonlinear Absorption Chromophores. *J. Chem. Phys.* **2002**, *117*, 7128−7136.

(76) Nasu, K.; Nakagawa, T.; Nomura, H.; Lin, C.-J.; Cheng, C.-H.; Tseng, M.-R.; Yasuda, T.; Adachi, C. A Highly Luminescent Spiro-Anthracenone-Based Organic Light-Emitting Diode Exhibiting Thermally Activated Delayed Fluorescence. *Chem. Commun.* **2013**, *49*, 10385−10387.

(77) Lakowicz, J. R., *Principles of Fluorescence Spectroscopy*. 2nd ed.; Kluwer Academic: New York, 1999.

(78) Uoyama, H.; Goushi, K.; Shizu, K.; Nomura, H.; Adachi, C. Highly Efficient Organic Light-Emitting Diodes from Delayed Fluorescence. *Nature* **2012**, *492*, 234−238.

(79) Nakagawa, T.; Ku, S.-Y.; Wong, K.-T.; Adachi, C. Electroluminescence Based on Thermally Activated Delayed Fluorescence Generated by a Spirobifluorene Donor-Acceptor Structure. *Chem. Commun.* **2012**, *48*, 9580−9582.

(80) Li, W.; Li, J.; Wang, F.; Gao, Z.; Zhang, S. Universal Host Materials for High-Efficiency Phosphorescent and Delayed-Fluorescence OLEDs. *ACS Appl. Mater. Interfaces* **2015**, *7*, 26206−26216.

(81) Lee, S. Y.; Yasuda, T.; Yang, Y. S.; Zhang, Q.; Adachi, C. Luminous Butterflies: Efficient Exciton Harvesting by Benzophenone Derivatives for Full-Color Delayed Fluorescence OLEDs. *Angew. Chem. Int. Ed.* **2014**, *53*, 6402–6406.

(82) Zhang, X.-F.; Yang, X. Photosensitizer That Selectively Generates Singlet Oxygen in Nonpolar Environments: Photophysical Mechanism and Efficiency for a Covalent Bodipy Dimer. *J. Phys. Chem. B* **2013**, *117*, 9050–9055.

(83) Zhang, X.-F.; Feng, N. Photoinduced Electron Transfer-Based Halogen-Free Photosensitizers: Covalent Meso-Aryl (Phenyl, Naphthyl, Anthryl, and Pyrenyl) as Electron Donors to Effectively Induce the Formation of the Excited Triplet State and Singlet Oxygen for Bodipy Compounds. *Chem. – Asian J.* **2017**, *12*, 2447–2456.

(84) Filatov, M. A.; Karuthedath, S.; Polestshuk, P. M.; Savoie, H.; Flanagan, K. J.; Sy, C.; Sitte, E.; Telitchko, M.; Laquai, F.; Boyle, R. W., et al. Generation of Triplet Excited States via Photoinduced Electron Transfer in *meso*-anthra-BODIPY: Fluorogenic Response toward Singlet Oxygen in Solution and in Vitro. *J. Am. Chem. Soc.* **2017**, *139*, 6282–6285.

(85) Wang, Z.; Zhao, J. Bodipy–Anthracene Dyads as Triplet Photosensitizers: Effect of Chromophore Orientation on Triplet-State Formation Efficiency and Application in Triplet-Triplet Annihilation Upconversion. *Org. Lett.* **2017**, *19*, 4492–4495.

(86) Chen, K.; Yang, W.; Wang, Z.; Iagatti, A.; Bussotti, L.; Foggi, P.; Ji, W.; Zhao, J.; Di Donato, M. Triplet Excited State of Bodipy Accessed by Charge Recombination and Its Application in Triplet-Triplet Annihilation Upconversion. *J. Phys. Chem. A* **2017**, *121*, 7550–7564.

(87) Geist, F.; Jackel, A.; Irmler, P.; Linseis, M.; Malzkuhn, S.; Kuss-Petermann, M.; Wenger, O. S.; Winter, R. F. Directing Energy Transfer in Panchromatic Platinum Complexes for Dual Vis–Near-IR or Dual Visible Emission from σ-Bonded Bodipy Dyes. *Inorg. Chem.* **2017**, *56*, 914–930.

(88) Zhou, J.; Chen, P.; Wang, X.; Wang, Y.; Wang, Y.; Li, F.; Yang, M.; Huang, Y.; Yu, J.; Lu, Z. Charge-Transfer-Featured Materials-Promising Hosts for Fabrication of Efficient OLEDs through Triplet Harvesting *via* Triplet Fusion. *Chem. Commun.* **2014**, *50*, 7586–7589.

(89) Xiong, X.; Song, F.; Sun, S.; Fan, J.; Peng, X. Red-Emissive Fluorescein Derivatives and Detection of Bovine Serum Albumin. *Asian J. Org. Chem.* **2013**, *2*, 145–149.

(90) Chen, Y.-L.; Li, S.-W.; Chi, Y.; Cheng, Y.-M.; Pu, S.-C.; Yeh, Y.-S.; Chou, P.-T. Switching Luminescent Properties in Osmium-Based B-Diketonate Complexes. *ChemPhysChem* **2005**, *6*, 2012–2017.

(91) Tanaka, H.; Shizu, K.; Nakanotani, H.; Adachi, C. Dual Intramolecular Charge-Transfer Fluorescence Derived from a Phenothiazine-Triphenyltriazine Derivative. *J. Phys. Chem. C* **2014**, *118*, 15985–15994.

(92) Druzhinin, S. I.; Galievsky, V. A.; Demeter, A.; Kovalenko, S. A.; Senyushkina, T.; Dubbaka, S. R.; Knochel, P.; Mayer, P.; Grosse, C.; Stalke, D., et al. Two-State Intramolecular Charge Transfer (ICT) with 3,5-Dimethyl-4-(dimethylamino)benzonitrile (MMD) and Its Meta-Isomer mMMD. Ground State Amino Twist Not Essential for ICT. *J. Phys. Chem. A* **2015**, *119*, 11820–11836.

(93) Li, J.; Qian, Y.; Xie, L.; Yi, Y.; Li, W.; Huang, W. From Dark TICT State to Emissive *quasi*-TICT State: The AIE Mechanism of *N*-(3-(benzo[*d*]oxazol-2-yl)phenyl)-4-*tert*-butylbenzamide. *J. Phys. Chem. C* **2015**, *119*, 2133–2141.

(94) Cui, X.; Zhao, J.; Lou, Z.; Li, S.; Wu, H.; Han, K.-l. Switching of the Triplet Excited State of Rhodamine/Naphthaleneimide Dyads: An Experimental and Theoretical Study. *J. Org. Chem.* **2015**, *80*, 568–581.

(95) Gosztola, D.; Niemczyk, M. P.; Svec, W.; Lukas, A. S.; Wasielewski, M. R. Excited Doublet States of Electrochemically Generated Aromatic Imide and Diimide Radical Anions. *J. Phys. Chem. A* **2000**, *104*, 6545–6551.

(96) Sun, D.; Rosokha, S. V.; Kochi, J. K. Donor−Acceptor (Electronic) Coupling in the Precursor Complex to Organic Electron Transfer: Intermolecular and Intramolecular Self-Exchange between Phenothiazine Redox Centers. *J. Am. Chem. Soc.* **2004**, *126*, 1388−1401.

(97) Lee, S.-H.; Chan, C. T.-L.; Wong, K. M.-C.; Lam, W. H.; Kwok, W.-M.; Yam, V. W.-W. Design and Synthesis of Bipyridine Platinum(II) Bisalkynyl Fullerene Donor–Chromophore–Acceptor Triads with Ultrafast Charge Separation. *J. Am. Chem. Soc.* **2014**, *136*, 10041−10052.

(98) Suneesh, C. V.; Gopidas, K. R. Long-Lived Photoinduced Charge Separation Due to the Inverted Region Effect in 1,6-Bis(phenylethynyl)pyrene−Phenothiazine Dyad. *J. Phys. Chem. C* **2010**, *114*, 18725−18734.

(99) Brouwer, A. M.; Frochot, C.; Gatti, F. G.; Leigh, D. A.; Mottier, L. c.; Paolucci, F.; Roffia, S.; Wurpel, G. W. H. Photoinduction of Fast, Reversible Translational Motion in a Hydrogen-Bonded Molecular Shuttle. *Science* **2001**, *291*, 2124–2128.

(100) Ogiwara, T.; Wakikawa, Y.; Ikoma, T. Mechanism of Intersystem Crossing of Thermally Activated Delayed Fluorescence Molecules. *J. Phys. Chem. A* **2015**, *119*, 3415–3418.

(101) Wiederrecht, G. P.; Svec, W. A.; Wasielewski, M. R.; Galili, T.; Levanon, H. Novel Mechanism for Triplet State Formation in Short Distance Covalently Linked Radical Ion Pairs. *J. Am. Chem. Soc.* **2000**, *122*, 9715–9722.

(102) Corvaja, C.; Franco, L.; Pasimeni, L.; Toffoletti, A. Time Resolved EPR of Triplet Excitons in Phenazine-TCNQ Charge Transfer Crystal. *Appl. Magn. Reson.* **1992**, *3*, 797−813.

(103) Jamie, G.; Monkman, A. P.; Penfold, T. J. The Importance of Vibronic Coupling for Efficient Reverse Intersystem Crossing in Thermally Activated Delayed Fluorescence Molecules. *ChemPhysChem* **2016**, *17*, 2956–2961.

(104) Terazima, M.; Yamauchi, S.; Hirota, N. Properties of the Short-Lived Triplet States of Pyridazine and 3,6-Dichloropyridazine Studied by a Time-Resolved EPR Method. *J. Chem. Phys.* **1986**, *84*, 3679−3687.

(105) Terazima, M.; Yamauchi, S.; Hirota, N. A Time-Resolved EPR Study of the Magnetic and Decay Properties of Short-Lived Non-Phosphorescent $^{3}n\pi^{*}$ Pyridazine. *Chem. Phys. Lett.* **1985**, *120*, 321–326.

TOC Graphic